Interferometric Measurement of Induced Birefringence in Polycrystalline ZnSe

BY

Patricia Govender
B Sc Hons(UKZN)

Submitted in partial fulfilment of the
requirements for the degree of
Master of Science
in the School of Physics
University of KwaZulu-Natal

PIETERMARITZBURG
JANUARY 2011

Acknowledgements

There are many people to whom I am grateful for their encouragement and assistance for the duration of the work completed here. I especially would like to thank the following people:

Dr V. W. Couling, for his wonderful patience during the assembly of the entire project, as well as his support and commitment throughout this work.

Mr G. Dewar, of the Electronics Centre, for constructing as well as repairing various electronic components used in the experiment. A special thanks for the construction of the feedback circuit which was a crucial part of the experimental arrangement.

Mr K. Penzhorn, Mr R. Sivraman and Mr A. Zulu of the Physics Technical Staff for assisting me in obtaining various apparatus as well as in setting up the experiment.

The CSIR's DPSS unit, for a masters bursary and for the encouragement and attention paid to my work.

To my parents, sister and Sherwin Moodley, for their constant support and for taking an interest in my work at all times.

Declaration

This dissertation describes the work undertaken at the School of Physics, University of KwaZulu-Natal (Pietermaritzburg), under the supervision of Dr V. W. Couling, between January 2008 and July 2010.

I declare the work reported in this dissertation to be my own research, unless specifically indicated to the contrary in the text. This thesis has not been submitted in any form for any degree or examination to any other university.

Signed: .....

On this ..... day of 2010

I hereby certify that this statement is correct

.....

Dr V. W. Couling

(SUPERVISOR)

Abstract

The aim of this research project was to assemble an apparatus capable of measuring field-induced birefringence in polycrystalline ZnSe. A Michelson interferometric apparatus was assembled, and care was taken to actively stabilize the interferometer against the effects of environmental noise by using electronic feedback techniques. This greatly enhanced the sensitivity of the interferometric measurements. In addition, the applied electric field was modulated, allowing sophisticated phase-sensitive detection techniques to be used to extract the induced birefringences.

Once assembled, the interferometer was tested using electric-field induced birefringence in a perspex sample, since there is Kerr-effect data in the literature against which to compare our measured quadratic electro-optic coefficients. The interferometer was then used to measure the quadratic electro-optic coefficients of polycrystalline ZnSe, these being, to the best of our knowledge, the first such measurements for this species.

The theory of electro-optic and photoelastic phenomena is comprehensively reviewed. This has permitted a critical discussion of the measured Kerr coefficients obtained in this project. It is demonstrated how quadratic electro-optic coefficients measured using the traditional technique of static polarimetry might include contributions arising from the linear electro-optic effect, these data being rendered suspect. In addition, suggestions are made as regards to the future possibilities for extending the apparatus to allow for direct measurement of stress-induced birefringences.

Contents

Chapter 1

Introduction

This thesis is concerned with the development of a Michelson interferometer for the measurement of the birefringences that can be induced in transparent, isotropic solid media. Such birefringences can be induced in an isotropic medium either by application of a stress (the photoelastic effect), or by application of an electric field (the electro-optic effect).

In this chapter, the historical discovery of these phenomena is briefly described, followed by a review of their theoretical underpinnings. Polarimetric birefringence measurement techniques are compared and contrasted with interferometric techniques. The aims and objectives of this project are then described.

Chapter 2 presents the theoretical basis of optical interferometry, especially as applied to the Michelson interferometer. Chapter 3 describes the Michelson interferometric apparatus used in this study, while chapter 4 presents the

experimental Kerr-effect data gathered for perspex (polymethylmethacrylate, PMMA) and polycrystalline ZnSe, together with a critical discussion of the extracted electro-optic coefficients.

1.1 A Review of Photoelastic and Electro-optic Phenomena

1.1.1 Photoelastic phenomena

In 1814, David Brewster began investigating the birefringence induced in glass by inhomogenous heating [1]. The following year he discovered the photoelastic effect, whereby the application of pressure to transparent solids was found to induce birefringence [2, 3]. He undertook a thorough investigation of the birefringence induced in isotropic media, arguing that a compressing stress would always produce a linear birefringence [4–6].

If a uniform mechanical stress σ is applied to an isotropic transparent medium of refractive index n, then the medium sustains a deformation described by the so-called piezo-optic (or stress-optic) coefficients π_{11} and π_{12} [7]. The induced birefringence $(n_{\parallel} - n_{\perp})$ may be related to the magnitude of the applied mechanical stress σ by means of the expression $(n_{\parallel} - n_{\perp}) = \frac{1}{2} n^3 (\pi_{12} - \pi_{11}) \sigma$ [7–14], where $n_{\parallel}$ and $n_{\perp}$ are the induced refractive indices parallel and perpendicular to the direction of the applied stress.

Photoelastic phenomena remain of interest since, in high-power laser systems, the mechanical stresses induced in the optical components can result in distortion of the light beam. These mechanical stresses can arise from a variety of sources, including residual stresses within the window blank, mounting stresses, thermally-induced stresses, as well as those stresses arising from pressure gradients, vibrations and tracking accelerations (see, for example, [15–20]). The photoelastic effect is also exploited in the photoelastic modulator, where the stress-induced birefringence allows for the polarization of light to be continuously varied [21–27]. The presence of photoelastic birefringence, and hence of a degradation in image quality, is also of significance in modern optical devices such as liquid crystal displays and optical disks which are constructed from polymer materials [28].

1.1.2 Electro-optic phenomena

In 1845 Michael Faraday discovered that a plane-polarized beam of light travelling through a transparent medium with a uniform magnetic field applied parallel to the beam's direction of propagation results in a rotation of the plane of polarization [29]. This discovery essentially gave birth to the branches of physics known as electro-optics and magneto-optics. Though Faraday continued his investigations into the relationships between light, electricity and magnetism, his apparatus lacked the sensitivity required to observe the many relationships that have since been established. It was left to other researchers to improve upon Faraday's apparatus, and discover new phenomena (including the Kerr, Zeeman and Cotton-Mouton effects).

In 1875, the Rev. John Kerr, attempting to improve upon Faraday's apparatus and techniques, observed that application of a uniform electric field to an isotropic medium causes it to become birefringent [30]. This induced birefringence is proportional to the square of the applied electric field (which is applied at right angles to the direction of propagation of the probing light beam), hence the name quadratic electro-optic effect, and it arises essentially through the field-induced re-orientation of induced and permanent electric moments. Kerr later related the induced birefringence $(n_{\parallel} - n_{\perp})$ to the magnitude of the applied electric field E through the expression $(n_{\parallel} - n_{\perp}) = \lambda K E^2$ [31], where $n_{\parallel}$ and $n_{\perp}$ are the refractive indices induced parallel and perpendicular to the applied field, λ is the wavelength of the light beam and K is the Kerr constant.

In 1883 Wilhelm Röntgen and August Kundt independently discovered the linear electro-optic effect, whereby light propagating perpendicular to a uniform electric field applied to crystalline quartz produced a birefringence linear in the field [32–35]. They mistakenly attributed this effect to photoelastic phenomena arising from the piezoelectric strain induced in (and hence deformation of) the quartz crystal by the applied electric field. It was Friedrich Pockels who succesfully distinguished between the linear electro-optic effect and the photoelastic phenomena through his investigations of quartz, tourmaline, potassium chlorate and Rochelle salt [36, 37].

As will be shown in the theoretical review of the electro-optic effect, materials

which possess a centre of symmetry (i.e. which belong to a centrosymmetric point group), and in particular materials which are isotropic, do not exhibit the Pockels effect. Hence glass, amorphous substances and liquids (with the notable exception of liquid crystals) do not exhibit the linear (first-order) electro-optic effect, and have as their leading effect the quadratic (second-order) electro-optic, or Kerr, effect. Even higher-order electro-optic effects can exist, but are typically much smaller in magnitude, and so are generally undetectable. All substances no matter their symmetry, even isotropic media, will display the Kerr effect.

Today, electro-optic materials find wide application in optical communications, optical signal processing, switches, modulaters and phase-shifters [7–14]. Much contemporary research focusses on finding matrials with as large an electro-optic response (whether linear or quadratic) as possible (see, for example, [38–40]).

1.2 The Theoretical Underpinnings of Photoelastic and Electro-optic Phenomena

1.2.1 The linear, or Pockels, electro-optic effect

The theory of the electro-optic effect found in most textbooks dealing with the optical properties of crystals involves describing the birefringence of a solid transparent sample in terms of an index ellipsoid [7–14]. In the electric

dipole approximation, where higher-order multipole contributions (i.e. electric quadrupole, magnetic dipole and higher) are neglected on the grounds of contributing negligibly, the electric displacement vector $\boldsymbol{D}$ in the presence of the oscillating light-wave fields $\boldsymbol{\mathscr{E}}$ and $\boldsymbol{\mathscr{B}}$ is, in tensor notation (where the convention of summation over repeated indices is observed),

$$D_i = \epsilon_0 \mathscr{E}_i + P_i, \tag{1.1}$$

where ϵ_0 is the permittivity of free space, and P_i is the electric dipole moment density

$$P_i = \epsilon_0 \, \chi_{ij} \mathscr{E}_j \tag{1.2}$$

with χ_{ij} the electric susceptibility tensor. (χ_{ij} plays a similar role for anisotropic matter in the bulk as the polarizability tensor α_{ij} does for a single molecule. For the special case of isotropic matter, χ_{ij} reduces to the scalar factor χ.) Equation 1.1 may be written as

$$D_i = \epsilon_{ij} \mathscr{E}_j \tag{1.3}$$

where the dielectric tensor ϵ_{ij} is

$$\epsilon_{ij} = \epsilon_0 \left(\delta_{ij} + \chi_{ij} \right), \tag{1.4}$$

δ_{ij} being the Kronecker delta.

It is assumed that the medium is homogeneous and non-absorbing (i.e. loss-less), and magnetically isotropic (i.e. optically inactive). The energy density for a polarized anisotropic medium is

$$U = \tfrac{1}{2}\boldsymbol{\mathscr{E}}.\boldsymbol{D}\,, \tag{1.5}$$

which, using equation 1.3, may be written

$$U = \tfrac{1}{2}\,\mathscr{E}_i\,\epsilon_{ij}\mathscr{E}_j\,. \tag{1.6}$$

The χ_{ij} tensor elements depend on the choice of orientation of Cartesian axes $O(x, y, z)$ relative to the crystal structure, and this may be exploited by choosing principal dielectric axes such that off-diagonal elements of χ_{ij} vanish. The energy density becomes

$$U = \frac{D_x^2}{2\epsilon_{xx}} + \frac{D_y^2}{2\epsilon_{yy}} + \frac{D_z^2}{2\epsilon_{zz}}\,. \tag{1.7}$$

Replacing $\boldsymbol{D}/\sqrt{2U}$ by $\boldsymbol{r} = (x, y, z)$, and defining the principal indices of refraction n_x, n_y and n_z by $n_i^2 = \epsilon_{ii}/\epsilon_0$ (where $i = x, y, z$), allows equation 1.7 to be written as

$$U = \frac{x^2}{n_x^2} + \frac{y^2}{n_y^2} + \frac{z^2}{n_z^2} = 1\,. \tag{1.8}$$

This is the equation of a general ellipsoid with major axes parallel to the x, y and z directions. This ellipsoid is known as the index ellipsoid, although it is sometimes called the optical indicatrix.

It is useful to define the impermeability tensor η_{ij} as

$$\eta_{ij} = \frac{\epsilon_0}{\epsilon_{ij}} \tag{1.9}$$

since the propagation of a beam of light in a crystal can be described completely in terms of this tensor. The quantum theory of solids reveals that the optical dielectric impermeability tensor is a function of the distribution of charges in a crystal. Application of a uniform electric field to the crystal will result in a redistribution of the bond charges, and can also possibly lead to a slight deformation of the ion lattice. The resulting change in the impermeability tensor is what is known as the electro-optic effect. The electro-optic coefficients are traditionally defined as

$$\eta_{ij}\left(\boldsymbol{E}\right) - \eta_{ij}\left(0\right) \;\equiv\; \Delta\eta_{ij} \;=\; r_{ijk}E_k + s_{ijkl}E_kE_l \tag{1.10}$$

where $\boldsymbol{E}$ is the applied electric field. The constants r_{ijk} are the linear, or Pockels, electro-optic coefficients, while s_{ijkl} are the quadratic, or Kerr, electro-optic coefficients. The series in equation 1.10 has been truncated, with terms higher than quadratic being omitted, since these higher-order effects are negligible in most applications.

To show that the linear electro-optic effect vanishes in media with centrosymmetric point groups, with the quadratic electro-optic effect becoming the dominant phenomenon, requires consideration of the effect of spatial inversion on a crystal. This is achieved by transforming a point at $\boldsymbol{r}$ in the crystal with respect to the centre of inversion to the position $-\boldsymbol{r}$. The linear electro-optic tensor r_{ijk} transforms under the inversion operation I as follows:

$$Ir_{ijk} = r'_{ijk} = -r_{ijk}. \tag{1.11}$$

However, because of the inversion symmetry of the material, any tensor property must be invariant under the inversion operation, so that

$$r'_{ijk} = r_{ijk}. \tag{1.12}$$

Equations 1.11 and 1.12 can simultaneously hold if and only if $r_{ijk} = 0$, so that the linear electro-optic effect must vanish in centrosymmetric media.

Since the materials investigated in this study, namely perspex (polymethylmethacrylate, PMMA) and polycrystalline ZnSe, are essentially centrosymmetric, their leading electro-optic effect is the Kerr effect, which is now described in detail. (The form of the linear electro-optic tensor r_{ijk} for all noncentrosymmetric crystal classes can be found, for example, in [7–14], together with tabulations of the linear electro-optic coefficients for a range of crystals.)

1.2.2 The quadratic, or Kerr, electro-optic effect

Unlike the linear electro-optic effect, the quadratic electro-optic effect exists in a medium with any symmetry. It is useful to introduce contracted, and hence abbreviated, indices for the quadratic electro-optic coefficient s_{ijkl} in equation 1.10, which can be written

$$s_{ijkl} = \frac{1}{2}\left(\frac{\partial^2 \eta_{ij}}{\partial E_k \partial E_l}\right)_{E=0}. \tag{1.13}$$

Since the order of partial differentiation is immaterial, the indices k and l can be permuted, as may the indices of the symmetric tensor η_{ij}, so that $s_{ijkl} = s_{jikl}$ and $s_{ijkl} = s_{ijlk}$. The indices are contracted as follows:

$$\begin{aligned} 1 &= (11), \\ 2 &= (22), \\ 3 &= (33), \\ 4 &= (23) = (32), \\ 5 &= (13) = (31), \\ 6 &= (12) = (21). \end{aligned} \tag{1.14}$$

If an optically isotropic medium is placed in a static electric field, it is principally the alignment of the molecules in the presence of the field that causes the medium to become birefringent. The isotropic medium, once in the presence of the field, now behaves as a uniaxial medium, the direction of the electric field defining the optic axis. It is convenient to choose the z-axis to be in the direction of the electric field. The form of the (contracted) quadratic electro-optic coefficients s_{ij} for an initially isotropic medium is (bearing in mind that $s_{13} = s_{23} = s_{12}$ and $s_{33} = s_{11}$)

$$s_{ij} = \begin{bmatrix} s_{11} & s_{12} & s_{12} & 0 & 0 & 0 \\ s_{12} & s_{11} & s_{12} & 0 & 0 & 0 \\ s_{12} & s_{12} & s_{11} & 0 & 0 & 0 \\ 0 & 0 & 0 & s_{44} & 0 & 0 \\ 0 & 0 & 0 & 0 & s_{44} & 0 \\ 0 & 0 & 0 & 0 & 0 & s_{44} \end{bmatrix}, \tag{1.15}$$

where $s_{44} = \frac{1}{2}(s_{11} - s_{12})$. The equation for the index ellipsoid of an optically isotropic medium in the presence of a static electric field E becomes

$$x^2\left(\frac{1}{n^2} + s_{12}E^2\right) + y^2\left(\frac{1}{n^2} + s_{12}E^2\right) + z^2\left(\frac{1}{n^2} + s_{11}E^2\right) = 1, \tag{1.16}$$

which may be written as

$$\frac{x^2 + y^2}{n_\perp^2} + \frac{z^2}{n_\parallel^2} = 1 \tag{1.17}$$

where the refractive index perpendicular to the electric field, $n_\perp$, is

$$n_\perp \;=\; n \;-\; \tfrac{1}{2}\, n^3 s_{12} E^2, \tag{1.18}$$

while the refractive index parallel to the field, $n_\parallel$, is

$$n_\parallel \;=\; n \;-\; \tfrac{1}{2}\, n^3 s_{11} E^2. \tag{1.19}$$

The difference in induced birefringence, $(n_\parallel - n_\perp)$, is

$$\left(n_\parallel - n_\perp\right) \;=\; \tfrac{1}{2}\, n^3 \left(s_{12} - s_{11}\right) E^2 \;=\; -n^3 s_{44} E^2. \tag{1.20}$$

Since

$$\left(n_\parallel - n_\perp\right) \;=\; K \lambda\, E^2, \tag{1.21}$$

where K is the Kerr constant and λ is the vacuum wavelength of the probing beam of light, the Kerr constant and the quadratic electro-optic coefficients of an isotropic medium are seen to be related by the expression

$$s_{44} = -\frac{K\lambda}{n^3}\ . \tag{1.22}$$

It is worth mentioning that tabulations of the form of the quadratic electro-optic coefficients for all of the crystal classes (the majority of which are

noncentrosymmetric), as well as of measured values of the coefficients for some particular crystals, are given in several textbooks [7–14].

1.2.3 The photoelastic (stress-optic) effect

Analagous to the electro-optic effects described in equation 1.10 (arising from the application of a uniform electric field to matter), the photoelastic effect in a medium arises when an applied mechanical stress results in a change in the optical impermeability tensor, $\Delta\eta_{ij}$. This effect occurs in all states of matter, and $\Delta\eta_{ij}$ is related to the stress tensor σ_{kl} by [7–14]

$$\Delta\eta_{ij} \;=\; \pi_{ijkl}\,\sigma_{kl}\,, \tag{1.23}$$

where the series has been truncated to omit higher-order terms involving powers of σ_{kl}, these terms usually contributing negligibly compared to the linear term. π_{ijkl} is the stress-optic (or piezo-optic) tensor, and since both η_{ij} and σ_{kl} are symmetric tensors, so that their respective indices can be permuted, the permutation symmetry of the stress-optic tensor π_{ijkl} is identical to that of the quadratic electro-optic tensor s_{ijkl}. This allows the contracted indices in equation 1.14 to be used to abbreviate the notation as done previously for s_{ijkl}, equation 1.23 becoming

$$\Delta\eta_i \;=\; \pi_{ij}\,\sigma_j\,, \quad i,j = 1,\,2,\,\cdots\,6\,. \tag{1.24}$$

Since our samples (amorphous perspex and polycrystalline ZnSe) are isotropic (in the bulk), the discussion here will be limited to isotropic media. When

such an isotropic medium of refractive index n is placed under a uniform stress in the z direction, the medium sustains a deformation that causes the medium to become birefringent. The isotropic medium, once in the presence of the stress field, becomes a uniaxial anisotropic medium, the direction of the field defining the optic axis. The form of the (contracted) stress-optic coefficients π_{ij} are identical to those of the quadratic electro-optic coefficients s_{ij} (for all crystal classes!), so that for an initially isotropic medium

$$\pi_{ij} = \begin{bmatrix} \pi_{11} & \pi_{12} & \pi_{12} & 0 & 0 & 0 \\ \pi_{12} & \pi_{11} & \pi_{12} & 0 & 0 & 0 \\ \pi_{12} & \pi_{12} & \pi_{11} & 0 & 0 & 0 \\ 0 & 0 & 0 & \pi_{44} & 0 & 0 \\ 0 & 0 & 0 & 0 & \pi_{44} & 0 \\ 0 & 0 & 0 & 0 & 0 & \pi_{44} \end{bmatrix}, \tag{1.25}$$

where $\pi_{44} = \frac{1}{2}(\pi_{11} - \pi_{12})$. The equation for the index ellipsoid of an optically isotropic medium in the presence of a static stress field σ becomes

$$x^2 \left(\frac{1}{n^2} + \pi_{12}\,\sigma\right) + y^2 \left(\frac{1}{n^2} + \pi_{12}\,\sigma\right) + z^2 \left(\frac{1}{n^2} + \pi_{11}\,\sigma\right) = 1, \tag{1.26}$$

which may be written as

$$\frac{x^2 + y^2}{n_\perp^2} + \frac{z^2}{n_\parallel^2} = 1 \tag{1.27}$$

where the refractive index perpendicular to the stress field, $n_\perp$, is

$$n_\perp \;=\; n \;-\; \tfrac{1}{2}\, n^3 \pi_{12}\, \sigma, \tag{1.28}$$

while the refractive index parallel to the field, $n_\parallel$, is

$$n_\parallel \;=\; n \;-\; \tfrac{1}{2}\, n^3 \pi_{11}\, \sigma. \tag{1.29}$$

The difference in induced birefringence, $(n_\parallel - n_\perp)$, is

$$\left(n_\parallel - n_\perp\right) \;=\; \tfrac{1}{2}\, n^3 \left(\pi_{12} - \pi_{11}\right) \sigma \;=\; -n^3 \pi_{44}\, \sigma. \tag{1.30}$$

The photoelastic effect has been measured in polycrystalline ZnSe at a wavelength of 632.8 nm, yielding stress-optic coefficients of $\pi_{11} = -1.48 \times 10^{-12}$ m^2 N^{-1} and $\pi_{12} = +0.22 \times 10^{-12}$ m^2 N^{-1} [17].

Attention is now turned to a review of the traditional polarimetric techniques for experimental measurement of induced birefringence.

1.3 Polarimetric Measurement of Induced Birefringences

The birefringence induced in a transparent, isotropic solid medium by an applied electric or stress field can be measured by an optical polarimeter [41],

which essentially comprises a crossed polarizer and analyzer between which the birefringent medium is placed, as shown in the schematic in Figure 1.1.

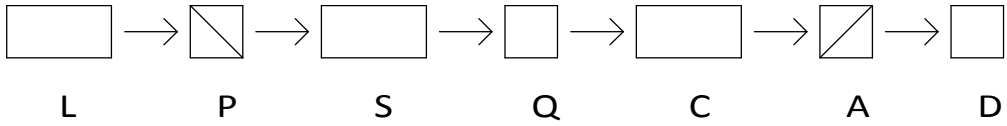

Figure 1.1: A schematic of an optical polarimeter used to measure field-induced birefringence in a solid medium: L, laser; P, polarizer; S, birefringent sample; Q, quarter-wave plate; C, compensator; A, analyzer; D, detector.

The observable property which is measured here is the optical retardation (or phase difference) ϕ arising due to the induced birefringence in the specimen. The space-fixed system of axes $\mathrm{O}(x, y, z)$ is fixed in the solid sample such that x is in the direction of propagation of the light beam, with z in the direction of the applied electric or stress field and y perpendicular to it. The azimuth of the linearly-polarized light beam is set by a polarizing prism to be 45° to the z-axis. When the field is applied, the component of the light beam vibrating in the xz plane will experience an induced refractive index $n_{\parallel}$ which differs from the induced refractive index $n_{\perp}$ experienced by the component vibrating in the xy plane. If the path-length traversed by the beam in the birefringent medium is l, then these two components will emerge from the specimen with a relative phase difference ϕ given by

$$\phi = \frac{2\pi l}{\lambda}(n_{\parallel} - n_{\perp})\,. \tag{1.31}$$

The emergent beam is elliptically polarized, but passing it through a quarter-wave plate with the fast axis set at 45° to the z-axis yields a linearly-polarized beam rotated from the 45° azimuth of the incident beam by $\phi/2$ radians. Since ϕ is typically a tiny angle, its precise measurement is best achieved by the technique of phase-sensitive detection, which requires modulation of ϕ (the dynamic polarimetric technique). Before the field is applied to the specimen, the analyzer in Figure 1.1 is crossed with the polarizer. Once the field is applied, the signal arriving at the detector due to ϕ is brought to a minimum value (null) by a compensating device placed between the quarter-wave plate and the analyzer. A Faraday rotator or a liquid Kerr cell could be used as a compensator, which is used to rotate the polarization plane of the light emerging from the quarter-wave plate by a variable but precisely-known angle, and so can rotate it back by $\phi/2$, bringing the detector signal to null.

In practice, achieving a null signal in this manner is problematic since the light intensity reaching the photodiode detector due to the induced birefringence will be too small to produce a signal that is discernible from the background noise. Instead, the linear method of optical detection of Badoz [42] can be utilized, whereby the optical signal is amplified by several orders of magnitude by introducing a static retardation into the optical train. This can be achieved by offsetting either the analyzer or quarter-wave plate by a small ($<1°$) angle ϵ. The phase-sensitive detector (psd) output can then be observed as the compensator is adjusted, null being achieved when there is zero psd output.

The more primitive static polarimetric technique does not modulate the applied field, which is instead static. Here, the rotation is nulled by a static rotation in the compensator. This method cannot make use of sophisticated phase-sensitive detection techniques (which can extract a small modulated signal buried in a great deal of noise), and so is much less sensitive. Experimental polarimetric arrangements where the polarizer and analyzer are not crossed are also used to extract electro-optic and stress-optic data. The theory of such arrangements is discussed in Born and Wolf [13].

Interferometric techniques have also been used to measure electro-optic and stress-optic phenomena. Here, the sample is placed in one arm of the interferometer. Once the induced birefringence is established in the sample (by application of an electric or stress field), the beam of light propagating through the sample undergoes a shift in phase, which in turn leads to a change in the intensity of the interference pattern which is formed where the reference and probing beams recombine. It is the measurement of this change in intensity that allows for the electro-optic or stress-optic coefficients to be measured.

Several interferometric set-ups have been reported in the literature [43−67], providing the basis for the experimental arrangement reported in this project. It should be noted that although the interferometric and the polarimetric techniques used in the measurement of electro-optic and stress-optic coefficients have comparable sensitivity, the interferometric technique has inherent advantages over the polarimetric one. Whereas the polarimetric method

determines the absolute value of the difference in coefficients, the interferometric method can reveal both the magnitude and sign of the individual coefficients. In addition, the static polarimetric technique cannot distinguish between birefringences induced by the linear and quadratic electro-optical effects, whereas both dynamic polarimetric and interferometric experimements can separate the two effects since they are modulated at different frequencies (the linear electro-optic effect at the frequency of the modulated field, the quadratic electro-optic effect at double this frequency).

The heterodyne interferometric technique is both more complicated and more expensive than the homodyne technique, and does not provide a dramatic improvement in sensitivity when measuring changes in optical path length [68−70], and so the heterodyne technique is not considered further in this work.

1.4 Aims and Objectives of this Project

The principal objective in this research project has been to assemble an interferometric apparatus capable of measuring field-induced birefringences in transparent, isotropic solid materials. The sample of particular interest has been polycrystalline ZnSe, which is used extensively, for example, in the optical components of high-power laser systems. The present research has focussed on measuring the extremely tiny quadratic electro-optic coefficients of ZnSe, since not only is this property of intrinsic interest, but this measurement demonstrates the feasibility of future extension of the project to

include the measurement of the stress-optic coefficients for this material. *In situ* measurement of the stress field in an optical component (via birefringence measurements) would ultimately permit measurement of the stresses induced by the mechanical mount, by thermal effects, mechanical vibrations, pressure gradients, and even by tracking accelerations, if required.

Since no previous measured values of the quadratic electro-optic coefficients for ZnSe could be found in the literature, it was desirable to also measure the coefficients for an isotropic species for which measured data from other techniques are available. This holds true for perspex (polymethylmethacrylate), there being several polarimetric studies of the Kerr effect reported in the literature. The interferometric measurements of the Kerr effect for perspex reported here have hence been critically compared against the polarimetric data to help gauge the performance of the current apparatus.

A future goal of this ongoing research is to use the interferometer developed in this project to measure stress-optic coefficients of optical materials (such as ZnSe). This could be achieved by the application of a modulated mechanical load to the samples (in place of the modulated electric field used here) to induce a modulated stress-induced birefringence. This modulated stress could be effected by means of a piezoelectric transducer element mounted against one of the sample faces in place of the electrodes used presently. A comprehensive knowledge of the electro-optic and stress-optic properties of this important optical material is a desirable goal, electro-optical materials finding wide application in optical communications, optical signal processing,

switches, modulaters and phase-shifters.

Bibliography

[1] D. Brewster, *Results of some recent experiments on the properties impressed upon light by the action of glass raised to different temperatures, and cooled under different circumstances*, Phil. Trans. R. Soc. Lond., **104**, 436 (1814)

[2] D. Brewster, *On the effects of simple pressure in producing that species of crystallization which forms two oppositely polarized images, and exhibits the complementary colours by polarized light*, Phil. Trans. R. Soc. Lond., **105**, 60 (1815)

[3] D. Brewster, *D. Nouvelles experiences sur la lumiere*, Bull. Sci. Soc. Philomath. Paris, 44 (1815)

[4] D. Brewster, *On new properties of heat, as exhibited in its propagation along plates of glass*, Phil. Trans. R. Soc. Lond., **106**, 46 (1816)

[5] D. Brewster, *On the communication of the structure of doubly-refracting crystals to glass, murite of soda, flour spar, and other substances by mechanical compression and dilation*, Phil. Trans. R. Soc. Lond., **106**, 156 (1816)

[6] D. Brewster, *On the laws which regulate the distribution of the polarizing force in plates, tubes, and cylinders of glass, that have received the polarizing structure*, Trans. Roy. Soc. Edinburgh, **8**, 353 (1818)

[7] J. F. Nye, *Physical Properties of Crystals*, (Clarendon Press: Oxford 1986)

[8] I. P. Kaminow, *An Introduction to Electrooptic Devices*, (Academic Press: New York 1974)

[9] A. Yariv and P. Yeh, *Optical Waves in Crystals*, (Wiley: New York 1984)

[10] A. Yariv and P. Yeh, *Quantum Electronics*, (Wiley: New York 1988)

[11] S. Huard, *Polarization of Light*, (Wiley: New York 1997)

[12] A. Yariv, *Optical Electronics in Modern Communications*, Clarendon Press: Oxford 1997)

[13] M. Born and E. Wolf, *Principles of Optics*, 7th (expanded) edition, (Cambridge University Press: Cambridge 2002)

[14] B. Kuhlow, *Landolt-Börnstein, Laser Fundamentals Part 2, Section 7.1: Modulators*, (Springer-Verlag: Berlin 2006), New Series Group VIII, Vol. 1A2

[15] D. T. F. Marple, *Refractive index of ZnSe, ZnTe, + CdTe*, J. Appl. Phys., **35**, 539 (1964)

[16] C. S. Chen, J. P. Szczesniak and J. C. Corelli, *Infrared stress birefringence in KBr, KCl, LiF and ZnSe*, J. Appl. Phys., **46**, 303 (1975)

[17] L. F. Goldstein, J. S. Thompson, J. B. Schroeder and J. E. Slattery, *Stress-optic coefficients of ZnSe*, Appl. Opt., **14**, 2432 (1975)

[18] A. Feldman, R. M. Waxler and D. Horowitz, in *Optical Properties of Highly Transparent Solids* edited by S. S. Mitra and B. Bendow, (Plenum: New York 1975), pg. 517

[19] A. Feldman, D. Horowitz, R. M. Waxler and M. J. Dodge, in *NBS Technical Note 993*, (U.S. GPO: Washington D.C. 1979), pg. 21

[20] G. R. Mariner and K. Vedam, *Stress-optic coefficient of ZnSe at 10.6 μm*, Appl. Opt., **20**, 2878 (1981)

[21] M. Hauser, L. S. Smith, D. G. Marlowe and P. R. Yoder, Jr., *The stressed-plate shutter, a new moderate-speed electro-optical light modulator*, Appl. Opt., **2**, 1172 (1963)

[22] M. Billardon and J. Badoz, *Modulateur de birefringence*, C. R. Seances Acad. Sci., Ser. B, **262**, 1672 (1966)

[23] F. Mollenauer, D. Downie, H. Engstrom and W. B. Grant, *Stress plate optical modulator for circular dichroism measurements*, Appl. Opt., **8**, 661 (1969)

[24] J. Kemp, *Piezo-optical birefringence modulators: A new use for a long-known effect*, J. Opt. Soc. Am. A, **59**, 950 (1969)

[25] T. Oakberg and A. Bryan, *Use of detectors with photoelastic modulators*, Proc. SPIE, **4819**, 98 (2002)

[26] B. Wang, R. R. Rockwell and A. Leadbetter, *A polarimeter using two photoelastic modulators*, Proc. SPIE, **5531**, 367 (2004)

[27] K. J. Braun, C. R. Lytle, J. A. Kavanaugh, J. A. thielen and A. S. Green, *A simple, inexpensive photoelastic modulator*, Am. J. Phys., **77**, 13 (2009)

[28] H. Shafiee, A. Tagaya and Y. Koike, *Mechanism of generation of photoelastic birefringence in methacrylate polymers for optical devices*, J. Polymer Sci. B, **48**, 2029 (2010)

[29] M. Faraday, *On the magnetization of light and the illumination of magnetic lines of force*, Phil. Trans. R. Soc. Lond., **136**, 1 (1946)

[30] J. Kerr, *A new relation between electricity and light: Dielectrified media birefringent*, Philos. Mag., Ser. 4, **50**, 336 (1875)

[31] J. Kerr, *Measurements and law in electro-optics*, Philos. Mag., Ser. 5, **9**, 157 (1880)

[32] W. C. Röntgen, *Über die durch electrische kräfte erzeugte änderung der doppelbrechung des quarzes*, Wied. Ann., **18**, 213 (1883)

[33] A. Kundt, *Über das optische verhalten des quarzes im electrischen felde*, Wied. Ann., **18**, 228 (1883)

[34] W. C. Röntgen, *Über die durch electrische kräfte erzeugte änderung der doppelbrechung des quarzes*, Wied. Ann., **18**, 534 (1883)

[35] W. C. Röntgen, *Bemerkung zu der abhandlung des Hrn. A. Kundt: "Über das optische verhalten des quarzes im electrischen feld"*, Wied. Ann., **19**, 319 (1883)

[36] F. Pockels, *Über den einfluss des electrostatischen feldes auf des optische verhalten piezoelectrischer krystalle*, Abhandl. Gesell. Wiss. Göttingen, **39**, 1 (1894)

[37] F. Pockels, *Lehrbuch der Kristalloptik*, (Teubner: Leipzig 1906)

[38] L. R. Dalton, *Rational design of organic electro-optic materials*, J. Phys.: Condens. Matter, **15**, R897 (2003)

[39] T. D. Kim, J. W. Kang, J. D. Luo, S. H. Jang, J. W. Ka, N. Tucker, J. B. Benedict, L. R. Dalton, T. Gray, R. M. Overney, D. H. Park, W. N. Herman and A. K. Y. Jen, *Ultralarge and thermally stable electro-optic activities from supramolecular self-assembled molecular glasses*, J. Am. Chem. Soc., **129**, 488 (2007)

[40] L. R. Dalton, S. J. Benight, L. E. Johnson, D. B. Knorr, I. Kosilkin, B. E. Eichinger, B. H. Robinson, A. K. Jen and E. E. Overney, *Systematic nanoengineering of soft matter organic electro-optic materials*, Chem. Mat., online advance article (2011)

[41] R. M. A. Azzam and N. M. Bashara, *Ellipsometry and Polarized Light*, (North Holland: New York 1977)

[42] J. Badoz, *Photoelectric measurements of weak birefringence and very small optical rotations*, J. Phys. Radium, **17**, 143A (1956)

[43] A. A. Fotchenkov, *Apparatus for measuring extremely small displacements of oscillating crystals*, Sov. Phys. Crystallogr., **2**, 643 (1957)

[44] I. S. Zheludev and A. A. Fotchenkov, *Electrostriction of linear dielectrics*, Sov. Phys. Crystallogr., **31**, 312 (1958)

[45] J. D. Zook, D. Chen and G. N. Otto, *Temperature dependence and model of electro-optic effect in* $LiNbO_3$, Appl. Phys. Lett., **11**, 159 (1967)

[46] Y. Fujii and T. Sakudo, *Interferometric determination of quadratic electro-optic coefficients in* $SrTiO_3$ *crystal*, J. Appl. Phys., **41**, 4188 (1970)

[47] S. Haussühl and G. Walda, *Measurement of absolute quadratic electro-optical effect in crystals LiF and* $\alpha - TlAl(SO_4)_2.12H_2O$, Phys. Stat. Sol., **5**, K163 (1971)

[48] K. Onuki, N. Uchida and T. Saku, *Interferometric method for measuring electro-optic coefficients in crystals*, J. Opt. Soc. Am., **62**, 1030 (1972)

[49] T. Kwaaitaal, *Contribution to the interferometric measurement of sub-Angstrom vibrations*, Rev. Sci. Instrum., **45**, 39 (1974)

[50] G. A. Massey, T. M. Loehr, L.J. Willis and J. C. Johnson, *Raman and electro-optic properties of potassium titanate phosphate*, Appl. Opt., **19**, 4136 (1980)

[51] K. Takizawa and M. Okada, *Simple method for measuring electro-optic coefficients by detecting the interference signal between transmitted and reflected beams*, J. Opt. Soc. Am., **72**, 809 (1982)

[52] B. J. Luymes, *Interferometric measurements of very small electrostrictive strains*, Rev. Sci. Instrum., **54**, 90 (1983)

[53] K. Takizawa and M. Okada, *Determination of relative signs of electro-optic and piezoelectric coefficients by measuring optical-phase shifts caused by an applied electric field*, J. Opt. Soc. Am. B, **2**, 289 (1985)

[54] J. D. Bierlein and C. B. Arweiler, *Electro-optic and dielectric properties of $KTiOPO_4$*, Appl. Phys. Lett., **49**, 917 (1986)

[55] Z. Y. Meng, T. Kwaaitaal and W. M. M. M. van den Eijnden, *The quadratic electrostrictive effect in CaF_2, SrF_2 and BaF_2 single-crystals*, J. Phys. D: Appl. Phys., **21**, 175 (1988)

[56] W. Y. Pan and S. J. Jang, *A sensitive modified Mach-Zehnder interferometer for studying electro-optic properties*, Rev. Sci. Instrum., **61**, 2109 (1990)

[57] B. L. Wang and X. Q. Liu, *Electro-optic tensor of $KTiOPO_4$ measured with a Fizeau interferometer*, Rev. Sci. Instrum., **63**, 5340 (1992)

[58] W. Kucharczyk, M. J. Gunning, R. E. Raab and C. Graham, *Interferometric investigation of the quadratic electro-optic effect in KDP*, Physica B, **212**, (1995)

[59] C. Z. Tan and J. Arndt, *Measurement of piezoelectricity in quartz and electrostriction in SiO_2-glass by interferometric method*, Physica B, **225**, 202 (1996)

[60] J. F. H. Nicholls, B. Bhenderson and B. H. T. Chai, *Accurate determination of the indices of refraction of nonlinear optical crystals*, Appl. Opt., **36**, 8587 (1997)

[61] T. Schubert, N. Haase, H. Kuck and R. Gottfried-Gottfried, *Refractive index measurements using an integrated Mach-Zehnder interferometer*, Sensors Actuators A, **60**, 108 (1997)

[62] M. J. Gunning, *Some experimental and theoretical studies in crystal optics*, Ph. D. thesis UKZN (1999)

[63] M. J. Gunning, R. E. Raab and W. Kucharczyk, *Interferometric measurements of electrostrictive coefficients of KDP and ADP in transmission*, Ferroelectr. Lett. Sect., **28**, (2001)

[64] M. Daimon and A. Masumuru, *High-accuracy measurements of the refractive index and its temperature coefficeint of calcium fluoride in a wide wavelength range from 138 to 2326 nm*, Appl. Opt., **41**, 5275 (2002)

[65] G. D. Gillen and S. Guha, *Refractive-index measurements of zinc germanium diphosphide at 300 and 77 K by use of a modified Michelson interferometer*, Appl. Opt., **43**, 2054 (2004)

[66] A. S. Andrushchak, B. V. Tybinka, I. P. Ostrovskij, W. Schranz and A. V. Kityk, *Automated interferometric technique for express ananlysis of the refractive indices in isotropic and anisotropic optical materials*, Opt. Laser Eng., **46**, 162 (2008)

[67] J. Zhang, J. Q. Xu, Ch. Y. Gao and Sh. Ch. Si, *Modified Michelson*

interferometer for probing refractive index of birefringent crystal, Opt. Laser Eng., **47**, 1212 (2009)

[68] A. Olsson, C. L. Tang and E. L. Green, *Active stabilization of a Michelson interferometer by an electro-optically tuned laser*, Appl. Opt., **29**, 1897 (1980)

[69] R. G. White and D. C. Emmony, *Active feedback stabilization of a Michelson interferometer using a flexure element*, J. Phys. E., **18**, 658 (1985)

[70] Y. J. Lin and C. J. Pan, *Precision displacement measurement by active laser heterodyne interferometry*, Appl. Opt., **30**, 1648 (1991)

Chapter 2

The Michelson Interferometer

2.1 Introduction

When an electric field is applied to an isotropic medium, a light wave propagating through it will experience a field-dependent change in optical path-length (ℓ) of $\Delta\ell$. This arises both from the Kerr effect (or quadratic electro-optic effect), which causes a change in refractive index, Δn, of the medium, as well as from the electrostrictive strain of the material, which changes its physical length by an amount ΔL. We have

$$\Delta\ell = L\Delta n + (n - n_a)\Delta L, \tag{2.1}$$

where L is the field-free length (through which the light traverses) of the material under investigation, n is the field-free refractive index of the material, and n_a is the refractive index of the medium (air in this study) surrounding the material.

Optical interferometry, being sensitive to very small changes in optical path-length, is the ideal means of measuring this field-induced change in optical path-length $\Delta\ell$. If the material is placed in one arm of an interferometer, the change in optical path-length would result in a shift in the phase of the interference pattern, allowing for precise determination of Δn. Since we are interested in measuring the difference in induced refractive indices parallel and perpendicular to the applied electric field, $n_{\parallel} - n_{\perp}$, the term $(n - n_a)\Delta L$ in equation 2.1 falls away, both the parallel and perpendicular polarization states experiencing the same electrostrictive dilation ΔL of the medium.

There are many examples in the literature of laser interferometric studies of birefringence changes arising due to the electro-optic effect (see, for example, [1-25] and the references therein), and the interferometers utilized are typically of the Mach-Zender and the Michelson type. The Michelson interferometer has one significant advantage over the Mach-Zender, in that the light wave which traverses the medium under investigation does so twice, hence amplifying the measured effect by a factor of two. Since the path-length changes induced by the applied electric field are typically very tiny (~ 1 Å), this doubling of the measured effect is a distinct advantage, and so the Michelson interferometer was employed in this study.

2.2 The Michelson Interferometer

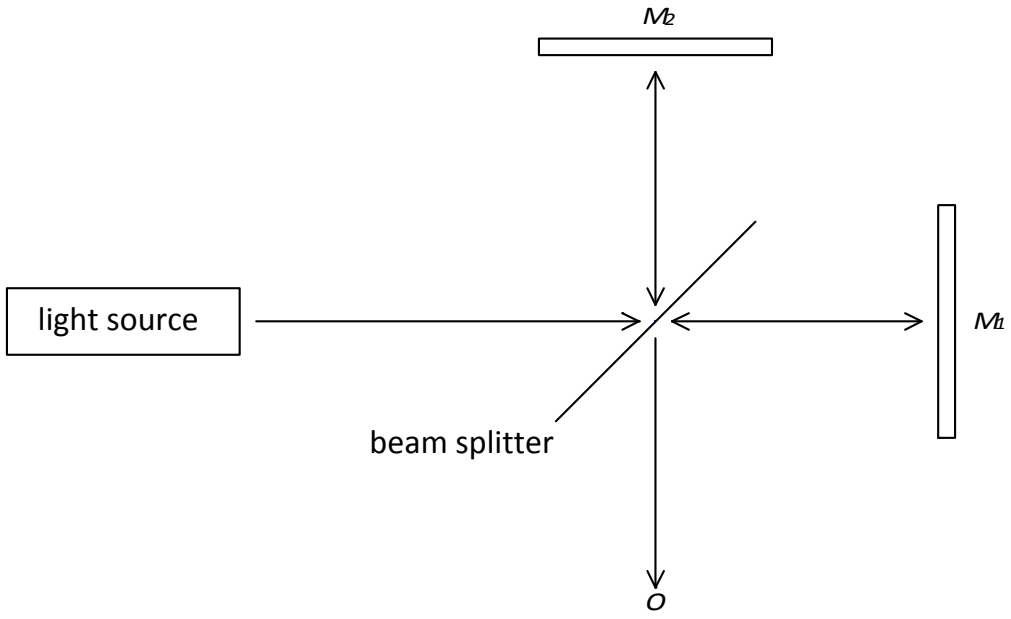

Figure 2.1: The Michelson interferometer arrangement.

The basic Michelson interferometer arrangement [26, 27] is shown in Figure 2.1. The Michelson interferometer functions as follows:

- A monochromatic light source emits a beam which is incident upon a 50% beam splitter.
- The beam splitter is orientated at 45° to the incident beam, splitting it into two coherent beams of equal intensity, and directing them along the two arms of the interferometer.
- One of these beams is transmitted through the beam splitter, and travels to mirror M_1, where it is reflected back to the beam splitter, being

deflected by 90° to a screen (or detector), O.

- The other beam is reflected by the beam splitter so that it travels to mirror M_2, where it is reflected back to the beam splitter, passing through it to reach the screen, O.

- At O the two beams are superimposed so that they can interfere with each other, and in so doing form interference fringes on the screen.

The intensity of the fringe pattern at O depends on the difference in optical path-length travelled by the two beams. This arises since the path-length difference affects the relative phase of the two waves, so that when they combine at O, the extent to which the two waves cancel affects the intensity.

The theoretical underpinnings of this interferometric approach are now presented in some detail.

2.3 Interferometric Theory

As shown by Born and Wolf [28], the resultant electric field $\boldsymbol{E}$ of the two interfering waves (linearly polarized in the same plane and travelling in the same direction) at a point with coordinate vector $\boldsymbol{r}$ is

$$\begin{aligned} \boldsymbol{E} &= \boldsymbol{E}_1 + \boldsymbol{E}_2 \\ &= e^{-i\omega n \boldsymbol{r}.\boldsymbol{\sigma}/c} \left(\boldsymbol{E}_1^{(0)} e^{i\phi_1} + \boldsymbol{E}_2^{(0)} e^{-i\phi_2} \right) \end{aligned} \tag{2.2}$$

where $\boldsymbol{\sigma}$ is the unit vector in the direction of propagation, which is along the wavefront normal; $\boldsymbol{E}_{\mathrm{j}}^{(0)}$ are the electric field amplitudes of the two light waves with ϕ_{j} their phase angles; c is the vacuum speed of light and n is the refractive index of the medium for the angular frequency ω of the light wave. From this, we can obtain the intensity of the combined waves at this point [28]:

$$\begin{aligned} I &= k\left|\boldsymbol{E}\right|^2 \\ &= k\left(\left|\boldsymbol{E}_1\right|^2 + \left|\boldsymbol{E}_2\right|^2 + 2\boldsymbol{E}_1\boldsymbol{E}_2\right) \\ &= I_1 + I_2 + 2\left(I_1 I_2\right)^{\frac{1}{2}} \cos\Delta\phi. \end{aligned} \tag{2.3}$$

Here, I_{j} represent the intensities of the two waves, $\Delta\phi$ is the optical phase-difference between them while k is a constant of proportionality. Since the interfering waves arise from a common source, the difference in the phase of the two waves is expressible in terms of the difference $\Delta\ell$ between the optical path-lengths travelled by the two waves at the point of interference. We obtain

$$\Delta\phi = \frac{2\pi\Delta\ell}{\lambda} \tag{2.4}$$

where λ is the vacuum wavelength of the light. Equations 2.3 and 2.4 yield the intensity I at a point on the resulting interference pattern expressed in terms of $\Delta\ell$ as

$$I = I_1 + I_2 + 2\,(I_1 I_2)^{\frac{1}{2}} \cos\left(\frac{2\pi\Delta\ell}{\lambda}\right). \tag{2.5}$$

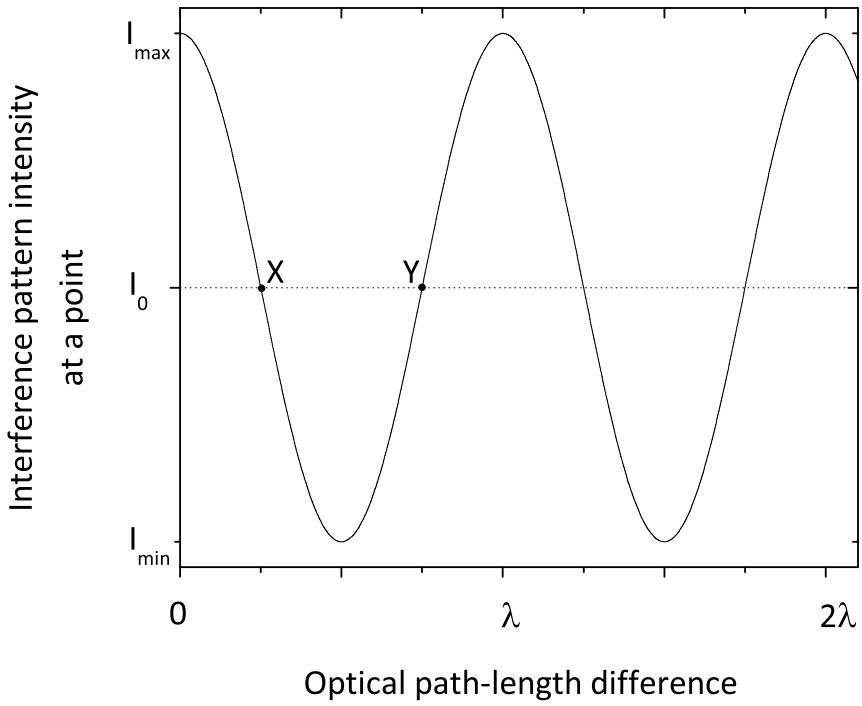

Figure 2.2: A plot of the variation in intensity at a point on the fringe pattern as a function of change in optical path-length, as given by equation 2.5.

This variation in the interference intensity at a point on the interference pattern as a function of change in optical path-length is plotted in Figure 2.2 Equation 2.5 is more conveniently expressed in terms of the maximum and

minimum intensities which appear in the interference pattern, these being, respectively, [28]

$$I_{\max} = I_1 + I_2 + 2\left(I_1 I_2\right)^{\frac{1}{2}} \tag{2.6}$$

for $\Delta\ell = n\lambda$, where $n = 0, 1, 2, \cdots$; and

$$I_{\min} = I_1 + I_2 - 2\left(I_1 I_2\right)^{\frac{1}{2}} \tag{2.7}$$

for $\Delta\ell = \frac{2n+1}{2}\lambda$, where where $n = 0, 1, 2, \cdots$.

Substituting these results into equation 2.3, we obtain the expression given by [29], namely

$$I = \tfrac{1}{2}\left(I_{\max} + I_{\min}\right) + \tfrac{1}{2}\left(I_{\max} - I_{\min}\right)\cos\left(\tfrac{2\pi\Delta\ell}{\lambda}\right). \tag{2.8}$$

The corresponding sensitivity of the intensity of the interfering beams at a point to small changes in the optical path-length difference, $\frac{\partial I}{\partial \Delta\ell}$, is

$$\frac{\partial I}{\partial \Delta\ell} = \left|\tfrac{\pi}{\lambda}\left(I_{\max} - I_{\min}\right)\sin\left(\tfrac{2\pi\Delta\ell}{\lambda}\right)\right|. \tag{2.9}$$

Hence, as the path-length difference $\Delta\ell$ changes, the sensitivity at a point in the interference pattern will vary between a maximum value of $\frac{\pi}{\lambda}\left(I_{\max} - I_{\min}\right)$

and a minimum value of zero. The point of maximum sensitivity corresponds to $\Delta\ell$ having values of

$$\Delta\ell = \tfrac{\lambda}{4}\,(2n+1), \text{ where } n = 0, 1, 2, \cdots \ . \tag{2.10}$$

Substituting these values of $\Delta\ell$ into equation 2.8 yields the interference pattern intensity at this point of maximum sensitivity as

$$I_0 = \tfrac{1}{2}\,(I_{\max} + I_{\min})\,. \tag{2.11}$$

Consequently, the point where the interferometer's interference pattern is the most sensitive to small changes in the optical path-length between the waves lies half way between the maximum and minimum intensities of the pattern (see, for example, points X and Y in Figure 2.2). Since the Michelson interferometer will be most sensitive to optical path-length changes at the points satisfying equation 2.11, it is ideal to operate the apparatus at these points for optimal results, and this will be borne in mind in the following chapters.

Operating the interferometer at a point of maximun sensitivity, and ensuring that the instrument is stable enough that the contribution made by environmental noises is negligible, the optical path-length difference is given by

$$\Delta\ell = \Delta\ell_{\text{effect}} + \tfrac{\lambda}{4}\,(2n+1)\,, \tag{2.12}$$

where $\Delta\ell_{\text{effect}}$ is the tiny change in optical path-length arising both due to the electric-field-induced quadratic electro-optic effect under investigation, and due to the electrostrictive strain induced in the sample. Substituting equation 2.12 into equation 2.8 we obtain

$$I = \tfrac{1}{2}\left(I_{\max} + I_{\min}\right) + \tfrac{1}{2}\left(I_{\max} - I_{\min}\right)\cos\left(\tfrac{2\pi}{\lambda}\left[\Delta\ell_{\text{effect}} + \tfrac{\lambda}{4}\left(2n+1\right)\right]\right). \quad (2.13)$$

Since $\cos\left(\frac{2\pi}{\lambda}\left[\Delta\ell_{\text{effect}} + \frac{\lambda}{4}\left(2n+1\right)\right]\right)$ simplifies to $\pm\sin\left(\frac{2\pi\Delta\ell_{\text{effect}}}{\lambda}\right)$, and since $\Delta\ell_{\text{effect}}$ is much smaller than the wavelength λ of the light being used to probe the sample, the approximation $\sin\left(\frac{2\pi\Delta\ell_{\text{effect}}}{\lambda}\right) \approx \frac{2\pi\Delta\ell_{\text{effect}}}{\lambda}$ may be used to good effect [30], equation 2.13 further simplifying to

$$I \approx \tfrac{1}{2}\left(I_{\max} + I_{\min}\right) \pm \left(I_{\max} - I_{\min}\right)\frac{\pi\Delta\ell_{\text{effect}}}{\lambda}. \quad (2.14)$$

Zhang *et al.* [30] have demonstrated that the above approximation is valid to within 1% for the He-Ne laser wavelength of 632.8 nm provided $\Delta\ell_{\text{effect}}$ does not exceed 13 nm. In equation 2.14, the first term, which is static, arises since the interferometer is operated at its most sensitive point, while the second term is a consequence of the optical path-length variations induced between the two superimposed light waves, and is seen to vary linearly with $\Delta\ell_{\text{effect}}$. The measured difference in intensity due to the effect being investigated is given by

$$\Delta I_{\text{effect}} = \pm\left(I_{\max} - I_{\min}\right)\left(\frac{\pi\Delta\ell_{\text{effect}}}{\lambda}\right). \quad (2.15)$$

Recasting equation 2.15 in terms of $\Delta\ell_{\text{effect}}$ yields [1]

$$|\Delta\ell_{\text{effect}}| = \frac{\lambda\Delta I_{\text{effect}}}{\pi\left(I_{\max} - I_{\min}\right)}. \tag{2.16}$$

From the above equation, it is apparent that, provided we know the wavelength of the light and the maximum and minimum intensities of the interference pattern, measurement of the change in light intensity of the interference pattern will allow for calculation of the induced optical path-length difference $\Delta\ell_{\text{effect}}$.

2.4 Electronic Stabilization of the Interferometer

Use of a photodiode detector to measure the intensity of the interference pattern greatly enhances the sensitivity of interferometric measurements, the optical signal being converted into an electronic signal, which, provided the signal has been suitably modulated, allows for the implementation of sophisticated phase-sensitive detection techniques. The Michelson interferometer is reported to have a theoretical sensitivity limit of 10^{-4} Å [31], where the limiting factor is the shot noise of the photodiode detector.

In practice this theoretical sensitivity limit is impossible to attain, owing to the effects of environmental noise on the interferometer. Environmental noise is generally low in frequency, and arises from a variety of sources, including

mechanical vibrations, thermal drift and field-induced strains, etc. Since the sensitivity of the interferometer is limited by these influences, it is essential that they be minimized, allowing the sensitivity limits of the instrument to approach the theoretical limit as closely as practically feasible.

Passive stabilization of the interferometer from mechanical vibrations can be achieved to an extent through resting it on a relatively massive table which is in turn supported by, though pneumatically isolated from, a base table. Such means of passive stabilization have been described, for example, by [32]. Minimization of thermal effects can be attempted through temperature-control of the environment. Such passive stabilization, which can be extremely costly to implement, is never entirely effective in isolating the interferometer from all noise, and this has led to the development of relatively cheap and effective active stabilization techniques.

Two distinct methods for the active stabilization of interferometers are utilized in most studies reported in the literature. Optical stabilization is employed in the so-called phase-quadrature interferometer originally proposed by Peck and Obetz [33]. This method proves to be inappropriate for our investigation, since it requires the introduction of a shift in phase between the two perpendicular components of the light in one arm of the interferometer, whereas we are passing linearly-polarized light through the samples to determine separately the refractive indices parallel and perpendicular to the applied electric field. We turn our attention instead to the electronic means of stabilization, which employs electronic feedback to mitigate against the

effects of low-frequency environmental noise.

The principles of the electronic stabilization of an interferometer have been described elsewhere [7], and are worth reviewing briefly. Consider a material which introduces an optical path-length change (much smaller in magnitude than the wavelength of the probing light) in one arm of an interferometer, via, for example, an induced effect such as the electric-field-induced electro-optic effect. It is possible to express the optical path-length difference between the two interfering waves as [32]

$$\Delta\ell = (\ell_1 - \ell_2) + \ell_{\text{effect}} + \ell_{\text{noise}} \tag{2.17}$$

where ℓ_1 and ℓ_2 are the respective static distances along the two arms of the interferometer, ℓ_{effect} is the small (and typically modulated) optical path-length change introduced by the effect under investigation, and ℓ_{noise} is the nett (dynamic) optical path-length variation due to all low-frequency noise contributions. By adjusting the static optical path-length difference such that the interferometer is being operated at a point of maximum sensitivity according to equation 2.10, we have

$$(\ell_1 - \ell_2) + \ell_{\text{noise}} = \tfrac{\lambda}{4}(2n+1), \text{ where } n = 0, 1, 2, \cdots . \tag{2.18}$$

Here the phase difference between the two interfering waves is given by

$$\Delta\phi = \tfrac{2\pi}{\lambda}\left\{(\ell_1 - \ell_2) + \ell_{\text{noise}}\right\} = \tfrac{\pi}{2}(2n+1), \text{ where } n = 0, 1, 2, \cdots . \tag{2.19}$$

The cumulative effect of this time-varying noise ℓ_{noise} will be to disturb the interferometer such that it cannot maintain balance at the point of maximum sensitivity, and will consequently compromise the accurate and precise measurement of ℓ_{effect}.

Electronic stabilization of the interferometer is concerned with cancelling, or at least minimizing, the noise contributions to the phase difference $\Delta\phi$ arising through the term ℓ_{noise}. Using a photodiode detector to monitor the light intensity at a point on the interference pattern yields a voltage signal which is proportional to the light intensity at the point. By measuring the photodiode output voltage corresponding to the light intensity at the point of maximum interferometer sensitivity, given by equation 2.11, it becomes possible to determine, through the drift in photodiode output voltage, the extent of the noise-induced drift from this point of maximum sensitivity. An active element in the interferometer can be continuously driven to compensate for this low-frequency drift, thereby actively maintaining the interferometer at its point of maximum sensitivity. The active element is typically a piezoelectric transducer or a condenser microphone which drives the mirror in the reference arm of the interferometer, thereby varying the reference arm's path length to compensate for the noise in equation 2.19 [7, 10, 14, 29, 30, 32, 34, 35]. Interferometeric measurement sensitivities of up to 10^{-3} Å have been achieved through this technique of electronic stabilization of the interferometer [7, 10].

For the interferometer used in this study, a piezoelectric transducer coupled

to a feedback circuit has been employed as the means of electronic stabilization. The reference-arm mirror was attached to this piezoelectric transducer. Further details are provided in Chapter 3.

Bibliography

[1] A. A. Fotchenkov, *Apparatus for measuring extremely small displacements of oscillating crystals*, Sov. Phys. Crystallogr., **2**, 643 (1957)

[2] I. S. Zheludev and A. A. Fotchenkov, *Electrostriction of linear dielectrics*, Sov. Phys. Crystallogr., **31**, 312 (1958)

[3] J. D. Zook, D. Chen and G. N. Otto, *Temperature dependence and model of electro-optic effect in* $LiNbO_3$, Appl. Phys. Lett., **11**, 159 (1967)

[4] Y. Fujii and T. Sakudo, *Interferometric determination of quadratic electro-optic coefficients in* $SrTiO_3$ *crystal*, J. Appl. Phys., **41**, 4188 (1970)

[5] S. Haussühl and G. Walda, *Measurement of absolute quadratic electro-optical effect in crystals LiF and* $\alpha - TlAl(SO_4)_2.12H_2O$, Phys. Stat. Sol., **5**, K163 (1971)

[6] K. Onuki, N. Uchida and T. Saku, *Interferometric method for measuring electro-optic coefficients in crystals*, J. Opt. Soc. Am., **62**, 1030 (1972)

[7] T. Kwaaitaal, *Contribution to the interferometric measurement of sub-Angstrom vibrations*, Rev. Sci. Instrum., **45**, 39 (1974)

[8] G. A. Massey, T. M. Loehr, L.J. Willis and J. C. Johnson, *Raman and electro-optic properties of potassium titanate phosphate*, Appl. Opt., **19**, 4136 (1980)

[9] K. Takizawa and M. Okada, *Simple method for measuring electro-optic coefficients by detecting the interference signal between transmitted and reflected beams*, J. Opt. Soc. Am., **72**, 809 (1982)

[10] B. J. Luymes, *Interferometric measurements of very small electrostrictive strains*, Rev. Sci. Instrum., **54**, 90 (1983)

[11] K. Takizawa and M. Okada, *Determination of relative signs of electro-optic and piezoelectric coefficients by measuring optical-phase shifts caused by an applied electric field*, J. Opt. Soc. Am. B, **2**, 289 (1985)

[12] J. D. Bierlein and C. B. Arweiler, *Electro-optic and dielectric properties of $KTiOPO_4$*, Appl. Phys. Lett., **49**, 917 (1986)

[13] Z. Y. Meng, T. Kwaaitaal and W. M. M. M. van den Eijnden, *The quadratic electrostrictive effect in CaF_2, SrF_2 and BaF_2 single-crystals*, J. Phys. D: Appl. Phys., **21**, 175 (1988)

[14] W. Y. Pan and S. J. Jang, *A sensitive modified Mach-Zehnder interferometer for studying electro-optic properties*, Rev. Sci. Instrum., **61**, 2109 (1990)

[15] B. L. Wang and X. Q. Liu, *Electro-optic tensor of $KTiOPO_4$ measured with a Fizeau interferometer*, Rev. Sci. Instrum., **63**, 5340 (1992)

[16] W. Kucharczyk, M. J. Gunning, R. E. Raab and C. Graham, *Interferometric investigation of the quadratic electro-optic effect in KDP*, Physica B, **212**, (1995)

[17] C. Z. Tan and J. Arndt, *Measurement of piezoelectricity in quartz and electrostriction in SiO_2-glass by interferometric method*, Physica B, **225**, 202 (1996)

[18] J. F. H. Nicholls, B. Bhenderson and B. H. T. Chai, *Accurate determination of the indices of refraction of nonlinear optical crystals*, Appl. Opt., **36**, 8587 (1997)

[19] T. Schubert, N. Haase, H. Kuck and R. Gottfried-Gottfried, *Refractive index measurements using an integrated Mach-Zehnder interferometer*, Sensors Actuators A, **60**, 108 (1997)

[20] M. J. Gunning, *Some experimental and theoretical studies in crystal optics*, Ph. D. thesis UKZN (1999)

[21] M. J. Gunning, R. E. Raab and W. Kucharczyk, *Interferometric measurements of electrostrictive coefficients of KDP and ADP in transmission*, Ferroelectr. Lett. Sect., **28**, (2001)

[22] M. Daimon and A. Masumuru, *High-accuracy measurements of the refractive index and its temperature coefficeint of calcium fluoride in a wide wavelength range from 138 to 2326 nm*, Appl. Opt., **41**, 5275 (2002)

[23] G. D. Gillen and S. Guha, *Refractive-index measurements of zinc germanium diphosphide at 300 and 77 K by use of a modified Michelson interferometer*, Appl. Opt., **43**, 2054 (2004)

[24] A. S. Andrushchak, B. V. Tybinka, I. P. Ostrovskij, W. Schranz and A. V. Kityk, *Automated interferometric technique for express ananlysis of the refractive indices in isotropic and anisotropic optical materials*, Opt. Laser Eng., **46**, 162 (2008)

[25] J. Zhang, J. Q. Xu, Ch. Y. Gao and Sh. Ch. Si, *Modified Michelson interferometer for probing refractive index of birefringent crystal*, Opt. Laser Eng., **47**, 1212 (2009)

[26] A. A. Michelson, *Relative motion of the Earth and the luminiferous ether*, Amer. J. Sci., **22**, 120 (1881)

[27] A. A. Michelson, *Interference phenomena in a new form of refractometer*, Phil. Mag., **13**, 236 (1882)

[28] M. Born and E. Wolf, *Principles of Optics*, 7th (expanded) edition, (Cambridge University Press: Cambridge 2002)

[29] W. Y. Pan and L. E. Cross, *A sensitive double beam laser interferometer for studying high-frequency piezoelectric and electrostrictive strains*, Rev. Sci. Instrum., **60**, 2701 (1989)

[30] Q. M. Zhang, W. Y. Pan and L. E. Cross, *Laser interferometer for the study of piezoelectric and electrostrictive strains*, J. Appl. Phys, **63**, 2492 (1988)

[31] S. Sizgoric and A. A. Gundjian, *An optical homodyne technique for measurement of amplitude and phase of sub-Angstrom ultrasonic vibrations*, Proc. IEEE, **57**, 1313 (1969)

[32] G. Doswell and H. Kunov, *Active stabilization system for a laser interferometer*, Rev. Sci. Instrum., **61**, 1986 (1990)

[33] E. R. Peck and S. W. Obetz, *Wavelength or length measurement by reversible fringe counting*, J. Opt. Soc. Am., **43**, 505 (1953)

[34] V. L. Vlasov and A. N. Medvedev, *Photoelectric stabilized interferometer for studying frequency-amplitude properties of piezotransformers*, Prib. Techn. Eksp. 1, 179 (1972)

[35] W. M. J. Haesen and T. Kwaaitaal, *Improvement in interferometric measurement of sub-Angstrom vibrations*, Rev. Sci. Instrum, **47**, 434 (1976)

Chapter 3

The Experimental Setup

3.1 The Measurement Technique

The observable property which is measured in this experiment is the electric-field-induced change in optical path-length in a transparent medium experienced by a light wave propagating through the medium at right angles to the applied field. Equation 2.1 relates the field-induced change in optical path-length to the change in refractive index of the medium, as well as to the physical change in length of the medium due to electrostrictive strain. The goal of the interferometric investigation is to measure the difference in induced refractive indices for light linearly polarized in a plane parallel and perpendicular to the applied electric field respectively, $n_{\parallel} - n_{\perp}$, and since the electrostrictive dilation of the medium is the same whether the transmitted beam is plane-polarized parallel or perpendicular to the applied electric field, this electrostriction term cancels out, and so need not be directly measured.

The means of measuring the small field-induced changes in optical path length is based on the method of compensation. Application of a modulating voltage to the parallel-plate electrodes between which are sandwiched the transparent sample under consideration leads to an ocsillating shift in optical path length of the beam propagating through the sample as a consequence of the quadratic electro-optic effect as well as the electrostrictive effect. This sample is placed in the probing arm of the Michelson interferometer, yielding an oscillating shift in the intensity of the interference pattern where the two beams recombine. Since both the electro-optic and the electrostrictive effects are quadratic in the applied field, the oscillating shift in the interference pattern will be at twice the frequency ω of the modulating voltage applied to the electrodes.

The compensating device is a piezoceramic plate upon which is mounted the probing-arm mirror of the interferometer. Application of a voltage to the conducting surfaces coating the plate yields a precisely reproducible piezoelectric response, so that the thickness of the ceramic plate (perpendicular to the coated plane faces) will vary accordingly. Since the piezoceramic plate is mounted on to the mirror holder, with a small layer of prespex providing insulation, any variation in the ceramic plate's thickness translates into a displacement of the mirror surface, and hence into a precisely-controlled change in the optical path length of the probing arm of the interferometer. Provided the magnitude of the displacement of the piezoceramic surface as a function of applied voltage has been accurately calibrated, the exact magnitude of the change in optical path length will be accurately measurable.

To compensate for the path-length variation induced in the sample by the oscillating electric field requires that the piezoceramic be modulated at the frequency of this variation (i.e. $2\,\omega$) and exactly in antiphase to it, hence moving the mirror to produce a path-length change in the interferometer arm to null the electro-optical effect. This requires that the amplitude of the nulling voltage applied to the piezoceramic be carefully adjusted until the intensity variation in the interference pattern arising from the electro-optical effect (and oscillating at a frequency of $2\,\omega$), as measured by a lock-in amplifier monitoring the output of a photodiode detector, is brought exactly to a null.

At this null point, the electro-optic path-length variation induced in the transparent sample, which is of unknown magnitude and sign, has exactly the same magnitude, and is exactly in antiphase to, the optical path-length variation introduced by the piezoceramic with attached mirror. Provided the piezoceramic has been carefully calibrated, so that the voltage applied to it yields precise knowledge of both the sign and magnitude of its change in induced path-length, it becomes possible to deduce the sign and magnitude of the path-length variation induced in the sample by the voltage applied to its electrodes.

Thus the interferometer can be used to measure the small changes in optical path-length, $\Delta\ell$, induced in the sample by the applied electric field for light plane-polarized both parallel and perpendicular to the applied field. Through

equation 2.1, the difference in induced refractive indices parallel and perpendicular to the applied electric field, $n_{\parallel} - n_{\perp}$, can be extracted.

The apparatus used in this research project is now presented.

3.2 The Michelson Interferometric Apparatus

Figure 3.1 provides a schematic diagram of the apparatus used in this study, including the optical and electronic components. These components are now discussed in detail.

3.2.1 The optical bench

The components of the Michelson interferometer were individually secured onto a heavy cast-iron optical bench. The bench comprised four arms secured together in the shape of a cross, with adjacent arms perpendicular to each other. All of the optical components of the interferometer were fastened onto this optical bench using stands with vertical and horizontal adjustment, hence providing the means for precise alignment of the components. The laser was secured with two such stands, while the two mirrors, the lens, the beam splitter and the photodiode were secured with one stand each. A photograph of the optical rail with optical components is provided in Figure 3.2.

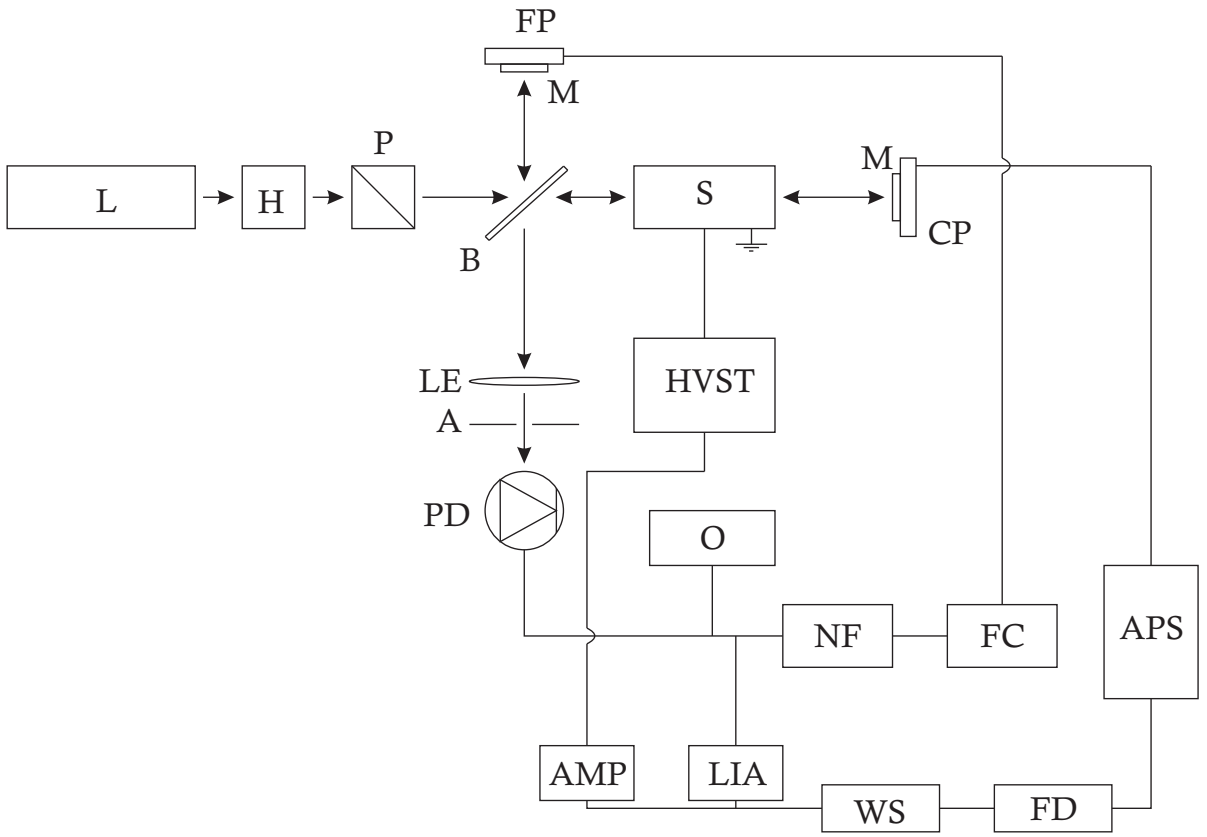

Figure 3.1: A schematic of the Michelson interferometric apparatus, including all optical and electronic components: L, laser; H, half-wave plate; P, polarizer; B, beam splitter; S, transparent sample (perspex and ZnSe); M, mirrors; FP, piezoelectric transducer feedback plate; CP, ceramic piezoelectric plate; LE, lens; A, aperture; PD, photodiode detector; O, oscilloscope; LIA, lock-in amplifier; NF, notch filter; FC, feedback circuit; WS, waveform synthesizer; FD, frequency doubler; APS, amplifier and phase shifter; AMP, high-voltage amplifier; HVST, high-voltage step-up transformer.

The optical bench with its components was placed on a heavy steel table which rested in turn upon eight inflated tyre tubes resting upon a concrete table. This arrangement served to isolate the optical table from environmental vibrations, thereby assisiting in the stabilization of the interferometer. All electronic equipment was placed either on the concrete table or on a workbench nearby in order to further isolate the Michelson interferometer from unnecessary sources of vibration or from the electric fields generated from these sources.

3.2.2 The laser

The laser used in this work was an Edmund Optical model 1145P He-Ne laser producing an almost completely linearly-polarized beam of wavelength 632.8 nm and maximum power *ca.* 22 mW. The laser was mounted via two stands, and carefully aligned such that the beam was travelling parallel with respect to the optical bench along each arm of the interferometer.

3.2.3 The half-wave plate and polarizer

Measurement of the birefringence induced in a specimen requires that the beam passing through it be a pure linearly polarized beam, the plane of polarization of which must be readily adjustable between a plane parallel to the applied electric field, and a plane perpendicular to it. This was achieved by passing the laser beam through a calcite Glan-Taylor polarizing prism

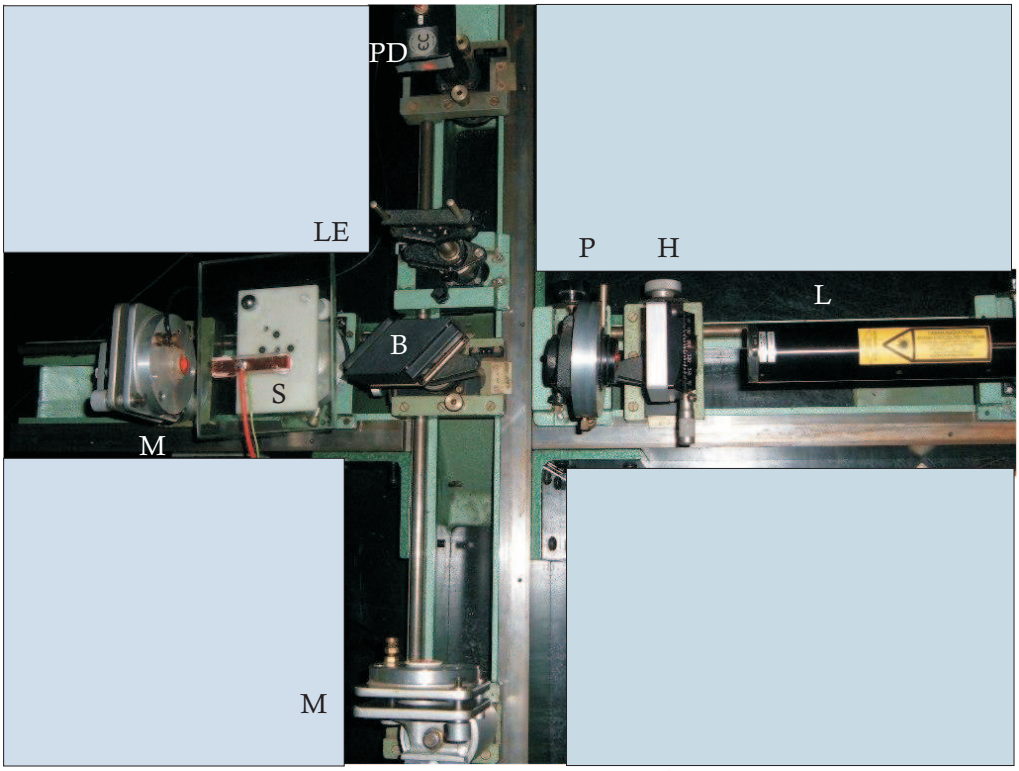

Figure 3.2: A photograph of the Michelson interferometer: L, laser; H, half-wave plate; P, polarizer; B, beam splitter; S, transparent sample (perspex here); M, mirrors; LE, lens; PD, photodiode detector.

(mounted in a precision rotator), the transmission axis of which was set to the desired polarization angle. A mica half-wave plate, also mounted in a precision rotator, was placed between the laser and the polarizer and oriented to rotate the plane of polarization of the laser beam to coincide with that of the polarizer, thereby maximizing the light intensity reaching the interferometer.

In order to establish the setting on the precision rotator (to better than $1'$ of

arc) such that the transmission axis of the polarizing prism was exactly vertical to the optical rail required the use of a second, reference, polarizing prism in a similar mount. Both prisms were then positioned on the optical rail, the laser beam passing centrally through each of them. The transmission axis of the polarizing prism was set to approximately vertical, and the reference prism was then rotated until the transmitted reference beam was completely extinguished, the setting on the divided circle α_1 being noted. The polarizing prism was then reversed by rotating it through 180° about a vertical axis, the reference prism again being adjusted for extinction at a setting α_2. The settings α_1 and α_2 will not be the same until the transmission axis of the polarizing prism is exactly vertical, this condition being achieved by rotating the polarizing prism through an angle $|\frac{1}{2}(\alpha_2 - \alpha_1)|$ and re-iterating the entire procedure until $\alpha_1 = \alpha_2$ to the required degree of precision.

3.2.4 The beam splitter and mirrors

A transparent plane-parallel glass plate served as the beam splitter, being partially silvered on one side so that close to 50% of the light would be transmitted down the reference arm of the interferometer, with the remaining *ca.* 50% being reflected down the other arm. To effect this, the beam splitter was placed at the intersection of the arms of the optical bench, and adjusted such that the laser beam impinging on it had an angle of incidence of 45°.

The transmitted beam was reflected off of a mirror in the reference arm back to the beam splitter, where it was then reflected and passed through a con-

verging lens (focal length 38 mm) to reach the photodiode detector. The beam which was initially reflected down the other arm of the interferometer was in turn reflected off a mirror in this probing arm, being directed back to the beam splitter, transmitting through it to pass through the converging lens and finally reach the photodiode detector. Both of the reflecting mirrors comprised flat glass plates which had been flash-coated with high-purity aluminium. In the probing arm of the interferometer, the mirror was mounted on the flat surface of a piezoelectric ceramic plate, while in the reference arm the mirror was mounted on a piezoelectric transducer. The purpose of each of these piezoelectric devices will be discussed shortly: suffice is to say that they were both mounted on adjustable holders with fine adjustment to allow the mirrors to be oriented such that their faces were perpendicular to the beams incident upon them. These holders could also translate along the optical rails, allowing the reference and probing-arm path-lengths to be set to match to within a few millimetres of each other.

3.2.5 The photodiode detector

The light beams emerging from the two arms of the interferometer were carefully oriented to superimpose at the aperture of a photodiode, thereby forming an interference pattern upon this measuring device. A silicon photodiode detector (UDT Sensors FIL100V0248) was used to convert the optical signal from the interference pattern into an electronic signal, the photodiode output voltage being proportional to the intensity of the light incident upon it. A piece of cardboard was placed over the aperture of the photodiode,

with a hole 1 mm in diameter providing a reduced aperture so that only the light from a small region of the interference pattern could be seen by the photodiode.

The spacing between adjacent fringes in the interference pattern was maximized both by adjusting the optical path-lengths to match as closely as possible, and by the action of a converging lens (focal length 38 mm) placed before the detector. The spacing between fringes was approximately 8 mm at the photodiode, and the 1 mm cardboard aperture ensured that this detector could only see a small portion of the interference pattern - a portion which would be of near-uniform intensity.

The output signal from the photodiode was monitored by an EG & G Princeton Applied Research model 5210 lock-in amplifier (LIA). Careful attention was paid to ensure that the screened co-axial cable connecting the photodiode output to the LIA was kept as far away from the other cables and electronic components as possible, thereby minimizing the introduction of noise via electromagnetic pickup.

The photodiode output signal was also simultaneously monitored by a Topward 20 MHz oscilloscope. The oscilloscope was also used to determine the maximum and minimum voltages of the input signal.

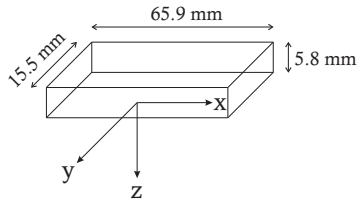

Figure 3.3: Schematic diagram of the birefringent specimens to indicate the space-fixed system of axes O(x,y,z).

3.2.6 Birefringent specimens

The specimens used for the measurement of electric-field-induced birefringence were perspex and pollycrystalline ZnSe, respectively. Both specimens were right-parallelepiped in shape, the perspex having dimensions of 65.9 mm $\times$ 15.5 mm $\times$ 5.8 mm (as shown in Figure 3.3, together with the space-fixed system of axes O(x,y,z)), and the ZnSe having dimensions 40.0 mm $\times$ 7.0 mm $\times$ 7.0 mm. The perspex was mechanically polished on all sides using aluminium oxide paste (Struers FF-Alumina suspension), with particular attention being paid to the polishing of the yz-plane faces since the light beam travels along the x-direction and enters the specimen via these faces. Strips of adhesive copper tape were attached along both of the xy-plane faces to provide the electrodes, with copper wires being soldered on to provide the means for applying a voltage.

The ZnSe polycrystalline sample was manufactured by Moltech using chemical vapour deposition, and was supplied with the yz-plane faces polished flat to within a wavelength (at 632.8 nm). Copper electrodes were attached as for the perspex sample.

Voltage was applied to the electrodes (typically 4 kV rms) using a high-voltage a.c. power supply in conjunction with a step-up transformer, both purpose-built by the University Electronics Centre. An Escort model EGC-3230 function generator was used to generate a sinusoidal signal of frequency 391 Hz, this frequency being chosen since it is both different from the mains 50 Hz (and its harmonics), and well below the mechanical resonance frequencies of the specimens. This signal of *ca.* 150 mV feeds the 125 W power amplifier (stable to $<0.1\%$) which drives a step-up transformer with a 1000:1 turns ratio. A second (step-down) transformer is used to monitor the high voltage applied to the sample's electrodes by means of a digital meter, and also serves to keep the output voltage constant by means of a feedback circuit.

The specimens were mounted on an insulating glass plate of dimensions 15.0 cm $\times$ 12.0 cm $\times$ 1.0 cm, this piece of glass being placed upon a perspex holder of dimensions 10.5 cm $\times$ 7.0 cm $\times$ 0.5 cm. This holder had adjustable nylon screws on two of the corners and a ballbearing on a third corner, hence allowing for precise alignment of the glass plate resting upon them, and hence of the specimen under investigation. The perspex holder was fixed to a stand similar to the ones holding the other optical components on the bench.

3.2.7 The piezoceramic compensator plate

A piezoceramic plate (diameter 16 mm and thickness 3 mm) with a reproducible and relatively large piezoelectric response provided the heart of the

compensating device in the probing arm of the interferometer. The plane-parallel faces of the plate were coated with conducting material, providing electrodes for the application of an electric field to the ceramic. The ceramic was securely attached to an adjustable holder, a layer of perspex providing insulation between the conducting surface and the holder. A small flat front-silvered mirror was attached to the other surface of the ceramic, providing the reflecting mirror for the interferometer's probing arm. The adjustable holder allowed for precise alignment of the mirror surface, which should be prependicular to the incident beam.

Application of a voltage to the electrodes of the ceramic plate yields a change in the plate thickness as a consequence of the piezoelectric response. This translates into a displacement of the mirror, and hence into a change in the optical path length in the probing arm of the interferometer. It is clearly essential that the relationship between applied voltage, $V^{\,\mathrm{comp}}$, and change in compensator plate thickness prependicular to the incident light, ΔL^{comp}, be accurately calibrated. This calibration was achieved by determining the ceramic's field-induced optical path-length changes by measuring the consequent change in intensity of the interference pattern of the interferometer when balanced at its most sensitive point (as discussed in section 2.3). The relationship between $V^{\,\mathrm{comp}}$ and ΔL^{comp} is given by

$$\Delta L^{\mathrm{comp}} = d\, V^{\,\mathrm{comp}}, \tag{3.1}$$

where d is the piezoelectric calibration constant. Application of a voltage to

the ceramic plate electrodes thus leads to a change in the optical path length of the probing arm of the interferometer of

$$\Delta\ell^{\,\mathrm{comp}} = 2\,\Delta L^{\mathrm{comp}} = 2\,d\,V^{\,\mathrm{comp}}, \tag{3.2}$$

which when substituted into equation 2.16 yields

$$|\Delta\ell^{\,\mathrm{comp}}| = 2\,d\,V^{\,\mathrm{comp}} = \frac{\lambda\,\Delta V}{\pi\,(V_{\mathrm{max}} - V_{\mathrm{min}})}\,. \tag{3.3}$$

Here, ΔV is the change in the photodiode detector output voltage (corresponding to the small change in intensity from that at the point of maximum stability) when the voltage $V^{\,\mathrm{comp}}$ is applied to the ceramic electrodes, while V_{max} and V_{min} are the maximum and minimum output voltages from the photodiode detector corresponding to the maximum and minimum intensities of the interference pattern in Figure 2.2.

By measuring ΔV for a range of ceramic electrode voltages $V^{\,\mathrm{comp}}$, it becomes possible, via equation 3.3, to obtain a precise value for the piezoelectric calibration constant d.

Once calibrated, the piezoceramic plate could be used to compensate for the quadratic electro-optic effect induced in the sample under investigation. This required that the ceramic plate be modulated at twice the frequency of the alternating voltage applied to the sample, this modulating voltage being variable in both amplitude and phase so that it could be set exactly

in antiphase to the electro-optic effect, and adjusted in amplitude to exactly null the effect. The plate voltage was derived from the same Escort waveform synthesizer driving the high-voltage a.c. power supply, necessitating that this branch of the supply voltage be passed through a frequency doubler and phase shifter

3.2.8 The piezoelectric transducer

To effect active electronic stabilization of the interferometer, as discussed in section 2.4, the mirror in the reference arm was mounted on a piezoelectric transducer, allowing it to be displaced by application of a voltage to the transducer electrodes. The transducer comprised a thin brass disc with a piezoceramic coating on one side. Application of a voltage across the piezoelectric device induced a stress within the ceramic, causing the brass disc to flex in either a concave or convex manner, depending on the polarity of the voltage. The transducer was attached to an adjustable holder, allowing the plane of the mirror to be adjusted perpendicular to the incident beam.

The electronic stabilization of the interferometer is now discussed in detail.

3.3 Electronic Stabilization of the Interferometer

The optical table for this experiment was designed to damp out as much mechanical and vibrational noise from the environment as possible. However,

even with the cushioning effect achieved by floating the table on inflated tyre tubes, a discernible slow drift was observed in the interference pattern. This was counteracted by a system of active stabilization achieved through electronic feedback. The components of this system are shown schematically in Figure 3.4.

The intensity at a point on the interference pattern as measured by the photodiode detector depends on the optical path-length difference $\Delta\ell$ between the interfering beams from the two arms of the interferometer, which, recall from equation 2.17, has three components:

$$\Delta\ell = (\ell_1 - \ell_2) + \ell_{\text{effect}} + \ell_{\text{noise}}. \tag{3.4}$$

Here, ℓ_1 and ℓ_2 are the static distances along either arm of the interferometer, ℓ_{effect} is the small modulated optical path-length change due to the electro-optic effect being measured, and ℓ_{noise} is the continuously (and randomly) fluctuating low-frequency ($<$10 Hz) noise signal.

The purpose of the electronic feedback control was to monitor the static (i.e. d.c.) output and the low-frequency noise output from the photodiode detector, and to maintain the d.c. component of the output at the point of maximum sensitivity for the interference pattern (as described by equation 2.11) while actively counteracting the low-frequency noise component. This was achieved through application of an appropriate voltage to the piezoelectric transducer, thereby translating the mirror in the reference arm of the interferometer and adjusting its optical path-length to compensate for, and hence eliminate, the effects of the noise signal.

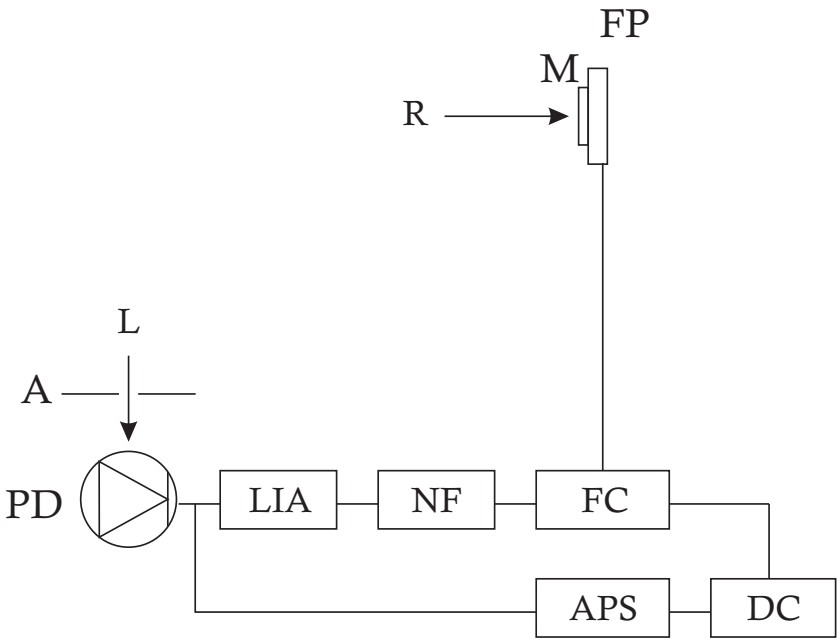

Figure 3.4: A schematic diagram of the optical and electronic components required in the active stabilization of the interferometer: L, light emerging from the interferometer; A, aperture; PD, photodiode detector; R, light beam in the reference arm of the interferometer; M, mirror; FP, feedback piezoelectric transducer plate; LIA, lock-in amplifier; NF, notch filter; FC, feedback circuit; APS, amplifier and phase shifter; DC, d.c. power.

Were the photodiode detector to pass the modulated signal arising from the quadratic electro-optic effect on to the feedback control, it would also attempt to null this measurement signal. To circumvent this, the output from the photodiode detector was initially passed through a tunable notch filter precisely tuned to filter out any signal ocsillating at the frequency of ℓ_{effect} (chosen as 782 Hz in this experiment). The notch filter was carefully de-

signed so as not to introduce any shift in the phase of the signal components oscillating at higher and lower frequencies than the 782 Hz, since this would adversely affect the ability of the feedback control to respond to noise fluctuations.

The circuit diagram of the feedback control, which was designed and built by the University Electronics Centre as part of this project, is shown in figure 3.5. Here, a variable d.c. reference signal is preset, and a differential amplifier is used to compare the low-frequency noise component of the photodiode detector output voltage agaist this d.c. reference. This yields a voltage which contains the difference between the d.c. reference and the d.c. photodiode output voltages, as well as a measure of the low-frequency noise in the photodiode output. This voltage is amplified and its phase inverted, after which it is applied to the piezoelectric transducer, causing a change in the optical path length in the interferometer's reference arm, and a corresponding change in the interference pattern intensity as seen by the photodiode detector. A feedback loop is thus established, serving to stabilize the interferometer when the difference between the d.c. reference and the d.c. photodiode output voltage is zero, and the low-frequency drift is cancelled out.

The dc reference voltage had to be initially adjusted to ensure that the portion of the interference pattern reaching the photodiode detector was that most sensitive to changes in optical path length, this being described at length in section 2.3. Initially, the optical path-length in the reference arm of the interferometer was modulated by precisely one wavelength by the ap-

plication of a sinusoidal voltage of fixed amplitude to the transducer element via the feedback circuit. The feedback circuit's dc reference voltage was then adjusted such that the photodiode signal (as viewed by an oscilloscope) varied sinusoidally, thus configuring the interferometer at its point of maximum sensitivity, the intensity of the interference pattern at this point being the $I_0 = \frac{1}{2}(I_{\max} + I_{\min})$ in equation 2.11.

The next chapter presents the results of the experimental investigations of the quadratic electro-optic effect undertaken using perspex and ZnSe samples.

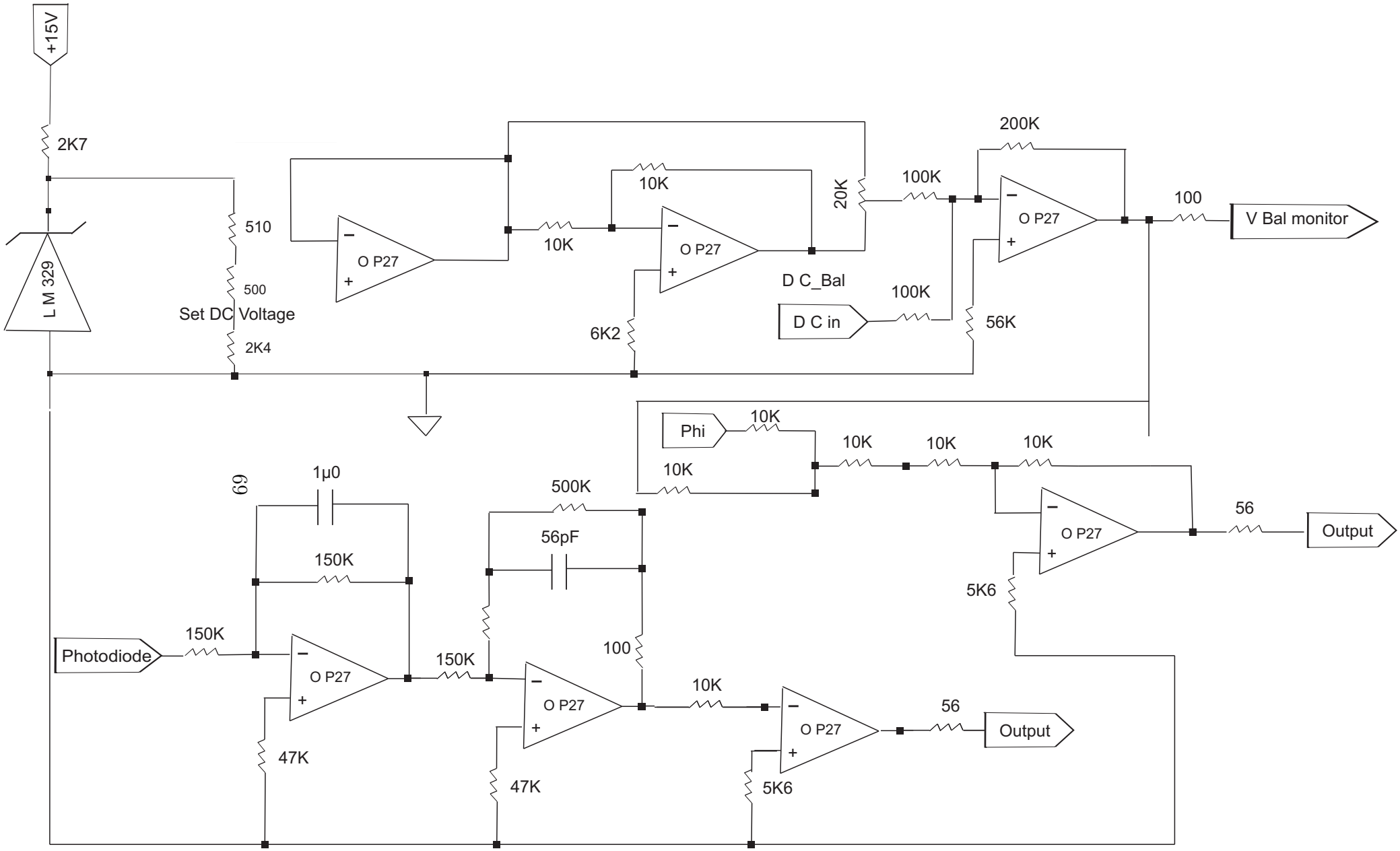

Figure 3.5: The circuit diagram for the feedback control

Chapter 4

Experimental Results and Discussion

4.1 Introduction

This chapter presents interferometric measurements of the quadratic electro-optic (Kerr) effect for two isotropic transparent media, namely perspex (polymethylmethacrylate) and polycrystalline ZnSe. The measurements have been undertaken using the apparatus developed in this research project, as described in the preceding two chapters.

In the first instance, the calibration of the piezoceramic compensating device is described. This is followed by the measured data of the quadratic electro-optic effect for perspex, for which there are published Kerr constants (obtained using static polarimetric techniques) against which to compare our measured value. The results are critically assessed. Finally, our measured

data for ZnSe are reported, this being, to the best of our knowledge, the first attempted measurement of the quadratic electro-optic coefficients for this species.

4.2 Determining the Calibration Constant d of the Piezoceramic Compensator Plate

In order to calibrate the piezoceramic compensator plate, the interferometric apparatus shown in Figure 3.1 was modified by removing the transparent sample and the high-voltage power supply. This calibration apparatus is represented by the schematic diagram in Figure 4.1. Just as described in the previous chapter for the Michelson interferometric apparatus (including transparent specimen in which birefringence is induced by application of a uniform electric field), the light intensity at a point on the interference pattern was measured by the photodiode detector, the output voltage of which was monitored both by the oscilloscope and the lock-in amplifier (LIA). Throughout the calibration procedure, the interferometer was operated at its point of maximum sensitivity, this point being maintained by the active electronic stabilization of the feedback control circuit.

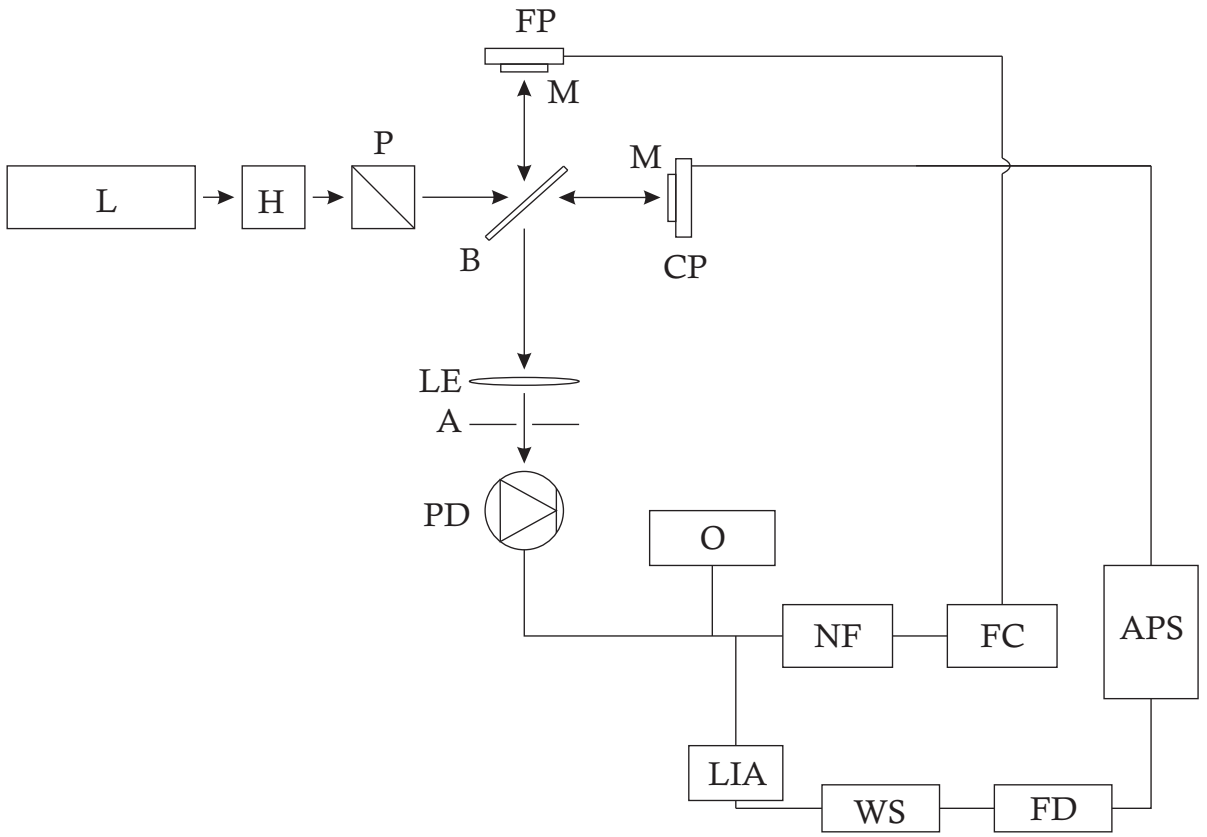

Figure 4.1: A schematic of the Michelson interferometric apparatus modified to perform the calibration of the piezoceramic compensator plate: L, laser; H, half-wave plate; P, polarizer; B, beam splitter; M, mirrors; piezoelectric transducer feedback plate; CP, FP, ceramic piezoelectric plate; LE, lens; A, aperture; PD, photodiode detector; O, oscilloscope; LIA, lock-in amplifier; NF, notch filter; FC, feedback circuit; WS, waveform synthesizer; FD, frequency doubler; APS, amplifier and phase shifter.

The oscilloscope was used to measure the difference between the maximum and minimum photodiode output voltages in equation 3.3, which correspond to the maximum and minimum interference pattern intensities in Figure 2.2. These maximum and minimum voltages arise when the interference pattern undergoes a shift of one complete fringe. To effect this shift of one complete fringe, a modulated voltage of frequency ω was applied to the piezoelectric transducer, the amplitude of this voltage being carefully chosen such that the mirror attached to the transducer element underwent a displacement matching a path-length shift in the reference arm of the interferometer of exactly one wavelength. The photodiode detector output was displayed on the oscilloscope, allowing the modulated output voltage (corresponding to the modulated intensity in the interference pattern) to be scrutinized, and for $(V_{\max} - V_{\min})$ to be accurately measured.

Once this measurement of $(V_{\max} - V_{\min})$ had been accomplished, the modulated signal of frequency ω was removed from the piezoelectric transducer, and a modulated voltage of frequency 2ω and of variable amplitude was applied instead to the piezoceramic compensator plate's electrodes by means of the frequency doubler, amplifier and phase shifter. (Calibrating the piezoceramic plate at the same frequency used when nulling the induced changes in path length averts the possibility of introducing any systematic error arising from frequency dependence in the piezoceramic response.) The photodiode output voltage was monitored by the LIA, enabling measurement of the small change induced in the photodiode signal by application of this modulated voltage to the piezoceramic element.

Table 4.1: A selected data set of change in photodiode detector output voltage ΔV as a function of applied piezoceramic plate voltage $V^{\,\mathrm{comp}}$ used to obtain the piezoceramic calibration constant d.

$V^{\,\mathrm{comp}}$/V	ΔV/mV
0.00	0.12
9.11	12.97
10.04	14.37
11.01	15.66
12.03	17.04
13.07	18.84
14.04	20.31
15.04	21.84
16.11	23.04
17.08	24.63
18.15	26.03
19.07	27.48

Measurements of the change in photodiode detector output voltage ΔV (as measured by the LIA) for voltages $V^{\,\mathrm{comp}}$ applied to the piezoceramic compensator plate electrodes ranging from zero to *ca.* 19 V were performed, and by plotting a least-squares regression of ΔV versus $V^{\,\mathrm{comp}}$, the calibration constant d was extracted from the best-fit slope via equation 3.3 and knowl-

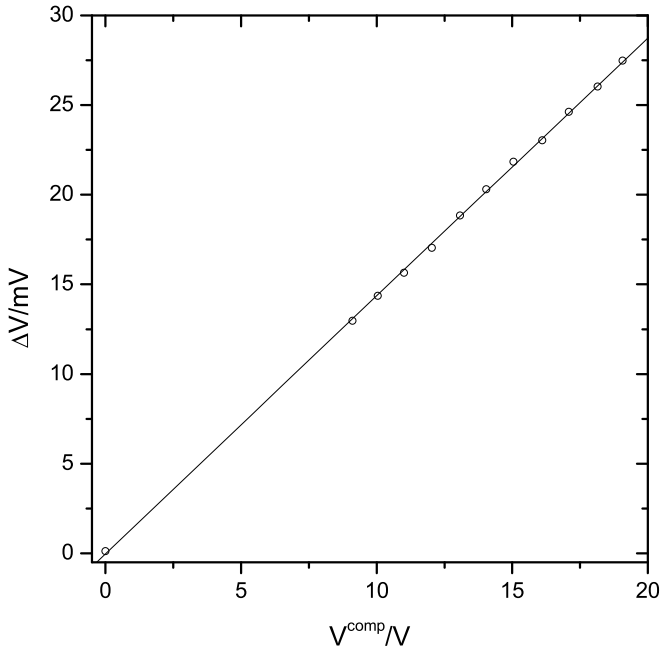

Figure 4.2: A plot of the ΔV versus $V^{\,\mathrm{comp}}$ data from Table 4.2, which is used to determine the calibration constant d for the piezoceramic compensator plate.

edge of both $(V_{\max} - V_{\min})$ and the vacuum wavelength $\lambda = 632.8$ nm of the light beam. A typical data set is provided in Table 4.2, and is shown plotted in Figure 4.2. Twenty separate such calibrations were performed during the course of this project, as tabulated in Table 4.2, together with the least-squares regression statistical uncertainty. These twenty calibration constants yield a mean value (and statistical standard error about the mean, σ_m) of $\overline{d} = (-3.077 \pm 0.016) \times 10^{-10}\ \mathrm{m\,V^{-1}}$. Since the uncertainty in d should also take

into account the uncertainties arising in the measurement of the various parameters in equation 3.3, including ΔV, $V^{\,\mathrm{comp}}$ and $(V_{\max} - V_{\min})$, this value becomes $\overline{d} = (-3.077 \pm 0.092) \times 10^{-10}\ \mathrm{m\,V^{-1}}$. The minus sign indicates that application of a positive voltage to the piezoceramic plate yields a decrease in plate thickness, and consequently an increase in the interferometer's reference arm path-length.

Table 4.2: Values obtained for the piezoceramic compensator plate calibration constant d as measured over the duration of this project.

$10^{10}\,d$ ($\mathrm{m\,V^{-1}}$)	$10^{10}\,d$ ($\mathrm{m\,V^{-1}}$)	$10^{10}\,d$ ($\mathrm{m\,V^{-1}}$)	$10^{10}\,d$ ($\mathrm{m\,V^{-1}}$)
-3.032 ± 0.039	-3.101 ± 0.033	-3.031 ± 0.103	-3.051 ± 0.079
-2.945 ± 0.043	-2.985 ± 0.046	-3.024 ± 0.030	-3.161 ± 0.047
-3.124 ± 0.029	-3.090 ± 0.013	-3.026 ± 0.025	-3.167 ± 0.060
-3.158 ± 0.039	-3.037 ± 0.035	-3.038 ± 0.023	-3.160 ± 0.030
-3.116 ± 0.066	-3.050 ± 0.047	-3.047 ± 0.017	-3.206 ± 0.023

4.3 The Quadratic Electro-optic (Kerr) Constant of Perspex

4.3.1 Results

The measurements for perspex (polymethylmethacrylate, PMMA) indicated that the reproducibility of the difference in induced refractive index, $n_{\parallel} - n_{\perp}$,

is such that any statistical variation in measured data is much smaller than the uncertainties in the variables, which include the piezoceramic compensator calibration constant, the compensator nulling voltage, the voltage applied to the electrodes, the electrode spacing and the length of the perspex specimen traversed by the light beam. (In fact, the principal contribution to the uncertainty in the experimentally deduced $n_{\parallel} - n_{\perp}$ values turns out to arise from the uncertainty in the compensator calibration constant, as will be demonstrated in due course.) Hence, the uncertainties quoted in this chapter will be those of the systematic errors in these measured variables.

Measurement of $n_{\parallel} - n_{\perp}$ is illustrated by means of one particular data set. Here, an rms voltage of 4.020 kV was applied to the perspex sample's electrodes, the modulated voltage having a frequency of 391 Hz. Since the quadratic electro-optic effect is quadratic in the applied field, the oscillating shift in optical path length of the beam traversing the perspex sample had a frequency of 782 Hz. The resultant oscillating shift in the intensity of the interference pattern was observed by the LIA, which monitored the output voltage of the photodiode detector. A compensating shift in optical path length in the probing arm of the interferometer was provided by passing a frequency-doubled (i.e. 782 Hz) modulated voltage, set to be precisely in antiphase to the path-length variation induced in the perspex specimen. The amplitude of this compensating voltage was carefully adjusted to exactly null the electro-optical effect.

The polarizing prism was initially set with its transmission axis vertical to

the optical rail, so that the linearly-polarized light beam had its plane of polarization set parallel to the applied electric field. The light wave propagating through the perspex medium experienced a field-induced change in optical path-length, $\Delta\ell_{\parallel}$, as given by equation 2.1:

$$\Delta\ell_{\parallel} = L\ n_{\parallel} + \text{const}, \tag{4.1}$$

where $n_{\parallel}$ is the *change induced* in the (field-free) refractive index parallel to the applied field, and where the constant represents the contribution to $\Delta\ell_{\parallel}$ arising from the electrostrictive strain induced in the perspex. Since const $= (n - n_a)\Delta L$ is independent of the plane of polarization of the light traversing the perspex sample, this contribution will ultimately cancel out, as shown shortly. The voltage required to compensate the induced Kerr effect was $V_{\parallel}^{\text{comp}} = -0.939$ V, yielding a $\Delta\ell_{\parallel} = \overline{d} \times V_{\parallel}^{\text{comp}}$ of $\Delta\ell_{\parallel} = (-3.077{\times}10^{-10})$ $\times$ (-0.939) m $= (2.890 \pm 0.089) \times 10^{-10}$ m. Here the uncertainty is the combined uncertainty of $\overline{d}$ and $V_{\parallel}^{\text{comp}}$.

The polarizing prism was subsequently adjusted such that its transmission axis was horizontal with respect to the optical rail, the light beam now having its plane of polarization set perpendicular to the applied field. The light wave propagating through the perspex medium now experienced a field-induced change in optical path-length, $\Delta\ell_{\perp}$, of

$$\Delta\ell_{\perp} = L\ n_{\perp} + \text{const}. \tag{4.2}$$

The compensating voltage was measured to be $V_{\perp}^{\text{comp}} = -0.775$ V, such that $\Delta\ell_{\perp} = \overline{d} \times V_{\perp}^{\text{comp}} = (-3.077 \times 10^{-10}) \times (-0.775)$ m $= (2.385 \pm 0.074) \times 10^{-10}$ m. From equations 4.1 and 4.3, it is immediately apparent that $(\Delta\ell_{\parallel} - \Delta\ell_{\perp})$ sees the cancellation of the constant term, const, arising from electrostrictive strain, such that

$$\left(\Delta\ell_{\parallel} - \Delta\ell_{\perp}\right) = L\left(n_{\parallel} - n_{\perp}\right). \tag{4.3}$$

Since the field-free length of the perspex specimen traversed by the light beam is $L = (6.592 \pm 0.002) \times 10^{-2}$ m, and bearing in mind that the beam travels twice through the specimen, we have

$$\left(n_{\parallel} - n_{\perp}\right) = \frac{\left(\Delta\ell_{\parallel} - \Delta\ell_{\perp}\right)}{2\,L} = (3.8 \pm 1.2) \times 10^{-10}. \tag{4.4}$$

The large uncertainty in $(n_{\parallel} - n_{\perp})$ of some 32% is an artefact of this quantity being a relatively tiny difference between two large numbers. To reduce this uncertainty, future work would have to concentrate on decreasing the uncertainty in the piezoceramic compensator plate's calibration constant d. This could be achieved in part by computer automation of the calibration process via use of an Agilent data-acquisition and control unit, whereby the voltage applied to the piezoceramic electrodes could be precisely varied, with the corresponding photodiode-detector response (as measured by the LIA) being recorded. Data could be gathered for several hours at a time, and statistically

analyzed by appropriate computer code, the large data sets thereby enabling the precision of the measured d to be increased. Of course, the uncertainty in the measured $(V_{\max} - V_{\min})$ in equation 3.3 is the predominant source of uncertainty in d, but by using a precision digital oscilloscope to perform this measurement, coupled with the computer-automated calibration procedure, it should be possible to increase the precision of d by around an order of magnitude.

Since the amplitude of the applied electric field is

$$E_0 = \frac{V_0}{s} = \frac{(4020 \pm 1) \times \sqrt{2}}{(0.581 \pm 0.002) \times 10^{-2}} = (9.785 \pm 0.036) \times 10^5 \ \mathrm{V\,m^{-1}},$$

where s is the spacing between electrodes, the Kerr constant K for perspex can be calculated using the equation

$$K = \frac{\left(n_{\parallel} - n_{\perp}\right)}{\lambda\, E_0^2} \tag{4.5}$$

to yield

$$K = \frac{(3.83 \pm 1.2) \times 10^{-10}}{632.8 \times 10^{-9} \times \left((9.785 \pm 0.036) \times 10^5\right)^2} = (6.3 \pm 2.0) \times 10^{-16}\,\mathrm{m\,V^{-2}}.$$

Perspex is an isotropic polymer medium, and the electric-field-induced birefringence is predominantly a consequence of partial alignment of the polymer

molecules in the presence of the field. For such a medium, the Kerr constant K is related to the quadratic electro-optic coefficients s_{11} and s_{22} [1–3] by

$$K = -\frac{n^3}{2\,\lambda}\,(s_{11} - s_{22})\,. \tag{4.6}$$

Hence, using a refractive index for perspex of $n = 1.489$ at 632.8 nm (interpolated from the dispersion data of Kasarova *et al.* in [4]), we obtain for the coefficient $s_{44} = \frac{1}{2}\,(s_{11} - s_{22})$ a value of $s_{44} = (-2.42 \pm 0.77) \times 10^{-22}\,\mathrm{m^2V^{-2}}$.

4.3.2 Discussion

Measurement of the Kerr effect in perspex was first reported in an article in the journal Nature in 1970 [5], though this paper was subsequently retracted on the grounds of a misinterpretation of the data. The work of Kim *et al.*, reported in 1983 [6], saw the measurement of the Kerr constant of perspex by means of a static ellipsometric study using light of wavelength 632.8 nm, which yielded a Kerr constant of $K \sim 2 \times 10^{-15}\,\mathrm{m\,V^{-2}}$. The 1991 investigation of Ishii and Griffis [7], also at a wavelength of 632.8 nm, employed a somewhat primitive static polarimeter, making use of a power meter as detector. Here the Kerr constant of perspex was found to be $K = 35.2 \times 10^{-15}\,\mathrm{m\,V^{-2}}$, a factor of 23 larger than that of Kim *et al.* The most recent study of the quadratic electro-optic effect in perspex reported in the literature appears to be that of Hartig *et al.* published in 1995 [8]. Here, once again, a static polarimetric apparatus is employed, using a He-Ne laser of quoted wavelength 633.2 nm. The Kerr constant for perspex is measured to be $K = 1.5 \times 10^{-15}\,\mathrm{m\,V^{-2}}$.

Our measured Kerr constant $K = (6.3 \pm 2.0) \times 10^{-16}\,\mathrm{m\,V^{-2}}$ for perspex is a factor of 2.4 smaller than the most recent literature value of Hartig *et al.* When comparing and contrasting these measured values, it should be borne in mind that Kucharczyk and Gorski [9, 10] have demonstrated that, for crystals whose symmetry properties possess a centre of inversion, and so which should not display the (relatively much larger) linear electro-optic effect, the quadratic electro-optic coefficients measured by static polarimetric techniques (i.e. where the applied electric field is static) can be up to two orders of magnitude larger than those obtained either by dynamic polarimetric or interferometric experiments. These differences are far too large to be accounted for by experimental measurement error, or by the temperature or wavelength dependence of the Kerr effect, or the frequency of the modulating electric field. They suggest, rather, that although theoretical conditions forbid the existence of the linear electro-optic effect, these stringent theoretical conditions might not be realized in practice, the crystal symmetry properties having physical imperfections that cause them to deviate slightly from the ideal case where there is a centre of inversion. Hence, in the static polarimetric measurements, where there is no means of distinguishing between the birefringence induced by the linear or the quadratic electro-optic effect, what is measured is in fact the combined response arising from both of these effects. Such results are clearly suspect, and yet the literature values predominantly reported for the quadratic electro-optic effect as measured in crystals which theoretically possess a centre of inversion are obtained using static polarimetric techniques.

The dynamic polarimetric and interferometric techniques both employ a modulated electric field, and here the linear electro-optic response is modulated at the same frequency as the applied field, while the quadratic electro-optic response is modulated at double the frequency of the applied field. By employing phase-sensitive detection techniques, where the photodiode detector signal is passed on to a lock-in amplifier, one is able to separate the two signals on account of their modulation frequencies being different, and so the danger of conflating the linear and quadratic responses is eliminated. Since our interferometric measurements make use of these sophisticated methods, there is no need to rely on dubious assumptions of the birefringent sample stringently possessing a centre of inversion, and hence of the linear electro-optic effect being entirely absent. Both perspex and polycrystalline ZnSe are assumed to be amorphous, and hence to be of the ∞m crystal class, possessing a centre of inversion. Such assumptions need not be strictly true, since in the manufacturing process of perspex, where the polymethylmethacrylate polymer sheets are formed by extrusion from the melt, the resulting sheet might not be perfectly amorphous. So too for polycrystalline ZnSe, where the CVD process results in minute (grain size *ca.* 50 μm) crystal fragments (ZnSe crystallizes into the zincblende structure belonging to the $\overline{4}$3m symmetry point group) which are assumed to deposit in a purely random orientation, whereas small systematic alignments may in fact occur, such that the polycrystalline sample may not be strictly amorphous, and hence may be capable of displaying a small linear electro-optic effect.

Indeed, the study of Kim *et al.* [6] reported the measurement via static polarimetric technique of the Kerr constant of perspex using 10 separate samples, K being found to range between 1.5 and 3.0 $\times 10^{-15}$ m V^{-2}. This variation in K is consistent with the presence of a linear electro-optic response that depends on the particular deviations from the ∞m point-group symmetry of each sample. Since, for crystals which are noncentrosymmetric, the linear electro-optic response is generally orders of magnitude larger than the quadratic response, even very small deviations in crystal symmetry from ∞m will lead to a non-negligible contribution to the induced birefringence. It is clear that static polarimetric determinations of the quadratic electro-optic effect are of questionable reliability, and that their results must be treated with caution.

One way of confirming that our interferometric Kerr constant for perspex is definitive would be to measure K for a range of perspex samples from various commercial manufacturers by means of our interferometric apparatus as well as by dynamic polarimetry. Setting up a dynamic polarimetric apparatus would constitute a new M Sc project in its own right, and is certainly worth the investment in time and money. It would also be possible, using either of the dynamic interferometric or polarimetric experiments, to measure the presence of a modulated linear electro-optic response, and to gauge the size of this contribution, thereby definitively addressing the extent to which this phenomenon is compromising the static polarimetric estimates of the quadratic electro-optic effect (in each unique perspex specimen). Such investigations would be time-consuming, and necessarily belong to future work,

being beyond the scope of the present investigation.

It should be noted that it is, in principle, possible to determine the individual contribution arising from electrostrictive strain for either of the induced refractive indices $n_{\parallel}$ or $n_{\perp}$ measured in this study. It is possible to exploit the presence of n_a, the refractive index of the medium surrounding the perspex sample (air in our measurements reported here), in equation 2.1. This term arises since the application of the electric field E results in an electrostrictive strain in the perspex, causing its physical length to change by ΔL. If the electric-field-induced birefringence of the perspex specimen were to be separately measured when surrounded by two different media of widely varying refractive index n_a, any discernible difference in $\Delta\ell$ (whether for light polarized parallel or perpendicular to the applied field) would arise purely as a result of the electrostrictive strain contribution, which could then be isolated. The change in length of the perspex specimen upon application of the electric field is given by

$$\Delta L \;=\; \gamma\, L\, E^2 \tag{4.7}$$

where L is the field-free length of the perspex specimen (traversed by the light beam) and where γ is the electrostrictive coefficient of the perspex. Knowledge of the electrostrictive strain contribution to either $\Delta\ell_{\parallel}$ or $\Delta\ell_{\perp}$ would then allow for the pure quadratic electro-optic effect contribution to each of $n_{\parallel}$ and $n_{\perp}$ to be extracted. Such experiements could be profitably explored in future work. It is worth emphasizing that it is impossible to

obtain such information from ellipsometric measurements (whether static or dynamic), which can only provide a measure of the difference in induced refractive indices $(n_{\parallel} - n_{\perp})$. Hence the inherent superiority of the interferometric technique over the ellipsometric.

4.4 The Quadratic Electro-optic (Kerr) Constant of Polycrystalline ZnSe

4.4.1 Results

With an rms voltage of 3.950 kV applied to the ZnSe sample's electrodes, and for vertically-polarized light, the compensating voltage was measured to be $V_{\parallel}^{\rm comp} = -0.249$ V, yielding $\Delta\ell_{\parallel} = \overline{d} \times V_{\parallel}^{\rm comp} = (0.766 \pm 0.026) \times 10^{-10}$ m. For horizontally polarized light, a compensating voltage of $V_{\perp}^{\rm comp} = -0.599$ V was obtained, such that $\Delta\ell_{\perp} = \overline{d} \times V_{\perp}^{\rm comp} = (1.843 \pm 0.057) \times 10^{-10}$ m.

The field-free length of the ZnSe specimen traversed by each pass of the light beam is $L = (3.997 \pm 0.002) \times 10^{-2}$ m, and again bearing in mind that the beam travels twice through the specimen, we have

$$\left(n_{\parallel} - n_{\perp}\right) \;=\; \frac{\left(\Delta\ell_{\parallel} - \Delta\ell_{\perp}\right)}{2\,L} \;=\; (-13.5 \pm 1.1) \times 10^{-10}. \qquad (4.8)$$

Here the more substantial difference in magnitudes of $n_{\parallel}$ and $n_{\perp}$, as compared

to PMMA, means that the uncertainty in $(n_{\parallel} - n_{\perp})$ is a somewhat smaller 8%.

The amplitude of the applied electric field is

$$E_0 = \frac{V_0}{s} = \frac{(3950 \pm 1) \times \sqrt{2}}{(0.704 \pm 0.002) \times 10^{-2}} = (7.935 \pm 0.025) \times 10^5 \ \mathrm{V\,m^{-1}},$$

and invoking the relationship

$$K = \frac{\left(n_{\parallel} - n_{\perp}\right)}{\lambda\, E_0^2} \tag{4.9}$$

between $n_{\parallel} - n_{\perp}$ and the Kerr constant K yields

$$K = \frac{(-13.5 \pm 1.1) \times 10^{-10}}{632.8 \times 10^{-9} \times \left((7.935 \pm 0.025) \times 10^5\right)^2} = (-33.9 \pm 3.0) \times 10^{-16}\,\mathrm{m\,V^{-2}}.$$

The refractive index of ZnSe is $n = 2.580$ at 632.8 nm [11], which, together with equation 4.6 allows the quadratic electro-optic coefficient $s_{44} = \frac{1}{2}(s_{11} - s_{22})$ to be extracted from the measured value for K, yielding a value of $s_{44} = (1.25 \pm 0.11) \times 10^{-22}\,\mathrm{m^2V^{-2}}$.

4.4.2 Discussion

To our knowledge, this is the first measurement of the quadratic electro-optic (Kerr) effect in polycrystalline ZnSe, so there are no measured data against which to compare our results. It is primarily for this reason that we have

also used our interferometric apparatus to measure the Kerr effect of perspex, since in this instance there are measured data (obtained via the technique of static polarimetry) against which to compare our findings. The dynamic interferometric measurements reported in this study are certainly more reliable than any obtained using static polarimetry, since the latter method does not discriminate between birefringence induced by the linear or the quadratic electro-optic effects.

4.5 Concluding Remarks

The Michelson interferometer assembled in this project has proved to be an effective means of measuring the Kerr constants of transparent solid media. Indeed, the main aim of the project was to assemble a dynamically-stabilized interferometer to measure induced birefringences in transparent solids, and to characterize its performance. This goal has been achieved, with the interferometer proving capable of measuring the relatively tiny quadratic electro-optic coefficients in transparent isotropic solids, while avoiding the inclusion of any contributions arising from the linear electro-optic effect that are unfortunately not discriminated against in static polarimetric measurements.

The Kerr constant obtained for perspex in this study is some 2.4 times smaller than that measured in the most recent static polarimetric investigation [8]. Since static polarimetric measurements are incapable of distinguishing between induced birefringence arising from the linear or the quadratic electro-

optic effects, we believe the results of Hartig *et al.* [8] to be unreliable, possibly including a non-negligible contribution arising from the Pockels effect. The sophisticated phase-sensitive detection techniques used in this work readily distinguish between the linear and the quadratic birefringences, so that considerable confidence can be placed in the Kerr constant reported here.

While the Kerr constants obtained for perspex and polycrystalline ZnSe are relatively tiny, both of these species could be of practical use in modern electro-optic devices. In addition, measurement of these relatively small electro-optic effects have provided a challenging test of the Michelson interferometer. These data are of intrinsic value, illustrating that the static polarimetric data gathered in the literature must be treated with caution. Now that the interferometer has been assembled, and its performance tested, it is possible to continue putting it to good use by characterizing the electro-optic response of new materials that potentially have larger electro-optic coefficients, making them ideal candidates for use in modern electro-optic devices.

A future goal of this ongoing research endeavour is to measure the stress-optic coefficients of ZnSe. Such measurements should be feasible using the current interferometer. This will require the application of a modulated mechanical load (in place of a modulated electric field) to the samples to induce a modulated stress-induced birefringence. For the samples used in this investigation, such a modulated load could be obtained by means of a piezoelectric transducer element mounted against one of the sample faces in place of the

electrodes used here. The frequency and amplitude of the applied stress will be variable, depending on the frequency and amplitude of the voltage applied to the piezoelectric transducer electrodes. The remainder of the interferometric apparatus and experimental technique will remain exactly the same as in the current project.

The stress-optic coefficients of ZnSe have already been well characterized [12–16], making it an ideal material for initial investigations, providing as it does a benchmark for the assessment of our interferometric technique. It should be noted that the stress-optic induced birefringence differences $n_{\parallel} - n_{\perp}$ for ZnSe in these experiments is typically of the order 10^{-4} to 10^{-5} (for optical path-lengths of around half a centimetre), which is much larger than our quadratic electro-optic induced birefringence difference for ZnSe of the order of 10^{-9}. It is immediately apparent that the application of much smaller loads will be possible in the interferometric study. Certainly, it should be possible to measure stress-optic coefficients arising in much thinner samples, such as in windows of less than a millimetre in thickness.

A more ambitious future goal is to measure the birefringences induced in optical materials *in situ*. The performance of high-power laser systems are often limited by the imperfections in their optical components. Such imperfections include the distortions induced by stresses arising from mechanical forces such as residual stresses within the material, stresses induced by the mechanical mount, thermally-induced stresses, as well as stresses arising from pressure gradients, mechanical vibrations and tracking accelerations (which

would be present if the laser were mounted in a rapidly accelerating projectile such as a rocket). It is clearly desirable to be able to measure the stress field in an optical component without having to demount it.

Bibliography

[1] J. F. Nye, *Physical Properties of Crystals*, (Clarendon Press: Oxford 1986)

[2] A. Yariv and P. Yeh, *Optical Waves in Crystals*, (Wiley: New York 1984)

[3] B. Kuhlow, *Landolt-Börnstein, Laser Fundamentals Part 2, Section 7.1: Modulators*, (Springer-Verlag: Berlin 2006), New Series Group VIII, Vol. 1A2

[4] S. F. Kasarova, N. G. Sultanova, C. D. Ivanov and I. D. Nikolov, *Analysis of the dispersion of optical plastic materials*, Opt. Mater., **29**, 1481 (2007)

[5] H. Pursey, *Kerr effect in polymers*, Nature, **227**, 834 (1970)

[6] K. S. Kim, T. C. Cheng and D. E. Cooper, *Kerr effect in solid polymethylmethacrylate and polyethylene*, J. Appl. Phys., **54**, 449 (1983)

[7] T. K. Ishii and A. Griffis, *Measurement of electro-optic effects in acrylic plastic*, Microwave and Opt. Tech. Lett., **4**, 387 (1991)

[8] C. Hartig, R. Kleppinger and B. J. Jungnickel, *Kerr-effect measurements on poly(vinylidine fluoride), poly(methyl methacrylate) and their blends*, Polymer, **36**, 4553 (1995)

[9] W. Kucharczyk and P. Gorski, *Measurement of non-linear electrooptic effects in KDP crystals*, Phys. Status Solidi A, **75**, K87 (1983)

[10] P. Gorski and W. Kucharczyk, *The quadratic electrooptic effect in KDP and ADP crystals*, Phys. Status Solidi A, **103**, K65 (1987)

[11] D. T. F. Marple, *Refractive index of ZnSe, ZnTe, + CdTe*, J. Appl. Phys., **35**, 539 (1964)

[12] C. S. Chen, J. P. Szczesniak and J. C. Corelli, *Infrared stress birefringence in KBr, KCl, LiF and ZnSe*, J. Appl. Phys., **46**, 303 (1975)

[13] L. F. Goldstein, J. S. Thompson, J. B. Schroeder and J. E. Slattery, *Stress-optic coefficients of ZnSe*, Appl. Opt., **14**, 2432 (1975)

[14] A. Feldman, R. M. Waxler and D. Horowitz, in *Optical Properties of Highly Transparent Solids* edited by S. S. Mitra and B. Bendow, (Plenum: New York 1975), pg. 517

[15] A. Feldman, D. Horowitz, R. M. Waxler and M. J. Dodge, in *NBS Technical Note 993*, (U.S. GPO: Washington D.C. 1979), pg. 21

[16] G. R. Mariner and K. Vedam, *Stress-optic coefficient of ZnSe at 10.6* μm, Appl. Opt., **20**, 2878 (1981)